Atmos. Chem. Phys. Discuss., doi:10.5194/acp-2016-1056, 2017
Manuscript under review for journal Atmos. Chem. Phys.
Discussion started: 7 March 2017

Simulating CH_4 and CO_2 over South and East Asia using the zoomed chemistry transport model LMDzINCA

Xin Lin[1], Philippe Ciais[1], Philippe Bousquet[1], Michel Ramonet[1], Yi Yin[1], Yves Balkanski[1], Anne Cozic[1], Marc Delmotte[1], Nikolaos Evangeliou[2], Nuggehalli K. Indira[3], Robin Locatelli[1a], Shushi Peng[4], Shilong Piao[4], Marielle Saunois[1], Panangady S. Swathi[3], Rong Wang[1], Camille Yver-Kwok[1], Yogesh K. Tiwari[5], Lingxi Zhou[6]

Affiliations:

[1]Laboratoire des Sciences du Climat et de l'Environnement, LSCE-IPSL (CEA-CNRS-UVSQ), Université Paris-Saclay, 91191 Gif-sur-Yvette, France

[2]Norwegian Institute for Air Research (NILU), Department of Atmospheric and Climate Research (ATMOS), Kjeller, Norway

[3]CSIR Fourth Paradigm Institute (formerly CSIR Centre for Mathematical Modelling and Computer Simulation), NAL Belur Campus, Bengaluru 560 037, India

[4]Sino-French Institute for Earth System Science, College of Urban and Environmental Sciences, Peking University, Beijing 100871, China

[5]Centre for Climate Change Research, Indian Institute of Tropical Meteorology, Pune, India

[6]Chinese Academy of Meteorological Sciences (CAMS), China Meteorological Administration (CMA), Beijing, China

Correspondence to: X. Lin (xin.lin@lsce.ipsl.fr)

[a] Now at: AXA Global P&C, Paris, France

Atmos. Chem. Phys. Discuss., doi:10.5194/acp-2016-1056, 2017
Manuscript under review for journal Atmos. Chem. Phys.
Discussion started: 7 March 2017

Abstract

The increasing availability of atmospheric measurements of greenhouse gases (GHGs) from surface stations can improve the retrieval of their fluxes at higher spatial and temporal resolutions by inversions, provided that chemistry transport models are able to properly represent the variability of concentrations observed at different stations. South and East Asia (SEA) is a region with large and very uncertain emissions of carbon dioxide (CO_2) and methane (CH_4), the most potent anthropogenic GHGs. Monitoring networks have expanded greatly during the past decade in this region, which should contribute to reducing uncertainties in estimates of regional GHG budgets. In this study, we simulate concentrations of CH_4 and CO_2 using a zoomed version of the global chemistry transport model LMDzINCA during the period 2006–2013. The zoomed version has a fine horizontal resolution of ~0.66° in longitude and ~0.51° in latitude over SEA and a coarser resolution elsewhere. The concentrations of CH_4 and CO_2 simulated from the zoomed model (abbreviated as 'ZASIA') are compared to those from the same model but with a uniform regular grid of 2.50° in longitude and 1.27° in latitude (abbreviated as 'REG'), both having the same vertical 19 sigma pressure levels and prescribed with the same biogenic and anthropogenic fluxes. Model performance is evaluated for annual gradients between sites, seasonal, synoptic and diurnal variations, against a new dataset including 30 surface stations over SEA and adjacent regions. Our results show that, when prescribed with identical surface fluxes, compared to REG, the ZASIA version moderately improves the representation of CH_4 mean annual gradients between stations as well as the seasonal and synoptic variations of this trace gas within the zoomed region. This moderate improvement probably results from reduction of representation errors and a better description of the CH_4 concentration gradients related to the skewed spatial distribution of surface CH_4 emissions, suggesting that the zoom transport model will be better suited for inversions of CH_4 fluxes in SEA. With the relatively coarse vertical resolution and low-frequency (monthly) prescribed fluxes, the model generally does not capture the diurnal cycle of CH_4 at most stations even with its zoomed configuration, emphasizing the need to increase the vertical resolution, and to improve parameterizations of turbulent diffusion in the planetary boundary layer and deep convection during the monsoon period. The model performance for CH_4 is better than that for CO_2 at any temporal scale, likely due to inaccuracies in the CO_2 fluxes prescribed in this study.

Atmos. Chem. Phys. Discuss., doi:10.5194/acp-2016-1056, 2017
Manuscript under review for journal Atmos. Chem. Phys.
Discussion started: 7 March 2017

Atmospheric Chemistry and Physics Discussions

1 Introduction

Despite attrition in the global network of greenhouse gas (GHG) monitoring stations (Houweling et al., 2012), new surface stations have been installed since the late 2000s in the northern industrialized continents such as Europe (e.g., Aalto et al., 2007; Biraud et al., 2000; Haszpra, 1995; Levin et al., 1995; Lopez et al., 2015; Popa et al., 2010), North America (e.g., Bakwin et al., 1998; Dlugokencky et al., 1995; Miles et al., 2012), and Northeast Asia (e.g., Fang et al., 2014; Sasakawa et al., 2010; Wada et al., 2011; Winderlich et al., 2010). In particular, the number of continuous monitoring stations over land has increased (e.g., Aalto et al., 2007; Bakwin et al., 1998; Lopez et al., 2015; Winderlich et al., 2010) given that more stable and precise instruments are available (e.g., Yver Kwok et al., 2015). These observations can be assimilated in inversion frameworks that combine them with a chemistry transport model and prior knowledge of fluxes to optimize GHG sources and sinks (Berchet et al., 2015; Bergamaschi et al., 2010, 2015, Bousquet et al., 2000, 2006; Bruhwiler et al., 2014; Gurney et al., 2002; Peters et al., 2010; Rödenbeck et al., 2003). Given the increasing observation availability, GHG budgets are expected to be retrieved at finer spatial and temporal resolutions by atmospheric inversions if the atmospheric GHG variability can be properly modeled at theses scales. A first step of any source optimization is to evaluate the ability of chemistry transport models to represent the variabilities of GHG concentrations, as transport errors are recognized as one of the main uncertainties in atmospheric inversions (Locatelli et al., 2013).

Many studies have investigated regional and local variations of atmospheric GHG concentrations using atmospheric chemistry transport models, with spatial resolutions ranging 100–300 km for global models (e.g., Chen and Prinn, 2005; Feng et al., 2011; Law et al., 1996; Patra et al., 2009a, 2009b) and 10–100 km for regional models (e.g., Aalto et al., 2006; Chevillard et al., 2002; Geels et al., 2004; Wang et al., 2007). Model intercomparison experiments showed that the atmospheric transport models with higher horizontal resolutions are more capable of capturing the observed short-term variability at continental sites (Geels et al., 2007; Law et al., 2008; Maksyutov et al., 2008; Patra et al., 2008; Saeki et al., 2013), due to reduction of representation errors (point measured versus gridbox-averaged modeled concentrations), improved model transport, and more detailed description of surface fluxes and topography (Patra et al., 2008). However, a higher horizontal model resolution also

Atmos. Chem. Phys. Discuss., doi:10.5194/acp-2016-1056, 2017
Manuscript under review for journal Atmos. Chem. Phys.
Discussion started: 7 March 2017

demands high-quality meteorological forcings and prescribed surface fluxes as boundary conditions (Locatelli et al., 2015).

Two main approaches have been deployed, in an Eulerian modeling context, to address the need for high-resolution transport modeling of long-lived GHGs. The first approach is to define a high-resolution grid mesh in a limited spatial domain of interest, and to nest it within a global model with varying degrees of sophistication to get boundary conditions for the GHGs advected inside/outside the regional domain (Bergamaschi et al., 2005, 2010; Krol et al., 2005; Peters et al., 2004). The second approach is to stretch the grid of a global model over a specific region (the so-called ‘zooming’) while maintaining all parameterizations consistent (Hourdin et al., 2006). For the former approach, several nested high-resolution zooms can be embedded into the same model (Krol et al., 2005) to focus on different regions. The ‘zooming’ approach has the advantage to avoid the nesting problems (e.g., tracers discontinuity, transport parameterization inconsistency) at the boundaries between a global and a regional model. In this study, we use the zooming capability of the LMDz model (Hourdin et al., 2006).

South and East Asia (hereafter ‘SEA’) has been the largest anthropogenic GHG emitting region since the mid 2000s due to its rapid socioeconomic development (Boden et al., 2015; Olivier et al., 2015; Le Quéré et al., 2015; Tian et al., 2016). Compared to Europe and North America where sources and sinks of GHGs are partly constrained by atmospheric observational networks, the quantification of regional GHG fluxes over SEA from atmospheric inversions remains uncertain because of the low density of surface observations (e.g., Patra et al., 2013; Swathi et al., 2013; Thompson et al., 2014, 2016). During the past decade, a number of new surface stations have been deployed (e.g., Fang et al., 2016, 2014; Ganesan et al., 2013; Lin et al., 2015; Tiwari and Kumar, 2012), which have the potential to provide new and useful constraints on estimates of GHG fluxes in this region. However, modeling GHG concentrations at these stations is challenging since they are often located in complex terrains (e.g. coasts or mountains) or close to large local sources of multiple origins. To fully take advantage of the new surface observations in SEA, forward modeling studies based on high-resolution transport models are needed to evaluate the ability of the inversion framework to assimilate such new observations.

Atmos. Chem. Phys. Discuss., doi:10.5194/acp-2016-1056, 2017
Manuscript under review for journal Atmos. Chem. Phys.
Discussion started: 7 March 2017

In this study, we apply the chemistry transport model LMDzINCA (Folberth et al., 2006; Hauglustaine et al., 2004; Hourdin et al., 2006; Szopa et al., 2013) zoomed down to a horizontal resolution of ~50km over SEA to simulate the variations of CH_4 and CO_2 during the period 2006–2013. The model performance is evaluated against observations from 20 flask and 13 continuous stations within and around the zoomed region. The variability of the observed or simulated concentrations at each station is decomposed for evaluation at different temporal scales, namely: the annual mean gradients between stations, the seasonal cycle, the synoptic variability and the diurnal cycle. For comparison, a non-zoomed version of the same transport model is also run with the same set of surface fluxes and the same vertical pressure levels, in order to estimate the improvement brought by the zoomed configuration. The detailed description of the observations and the chemistry transport model is presented in Section 2, together with the prescribed CH_4 and CO_2 surface fluxes that force the simulations, as well as the metrics used to quantify the model performance. An evaluation of the simulations performed is presented and discussed in Section 3, showing capabilities of the transport model to representthe annual gradients between stations, and the seasonal, synoptic, and diurnal variations. Conclusions and implications drawn from this study are given in Section 4.

2 Data and Methods

2.1 Model description

2.1.1 LMDzINCA

The LMDzINCA model couples a general circulation model developed at the Laboratoire de Météorologie Dynamique (LMD; Hourdin et al., 2006), and a global chemistry and aerosol model INteractions between Chemistry and Aerosols (INCA; Folberth et al., 2006; Hauglustaine et al., 2004). A more recent description of LMDzINCA is presented in Szopa et al. (2013). To simulate CH_4 and CO_2 concentrations, we run a regular version of the model with a horizontal resolution of 2.5° (i.e., 144 model grids) in longitude and 1.27° (i.e., 142 model grids) in latitude (hereafter this version is abbreviated as 'REG') and a zoomed version with the same number of grid boxes, but a resolution of ~0.66° in longitude and ~0.51° in latitude in a region of 50–130°E and 0–55°N centered over India and China (hereafter this version is abbreviated as 'ZASIA') (Figure 1; see also Wang et al., 2014, 2016). It means that, in terms of the surface area, a gridcell from REG roughly contains 9 grid-cells from ZASIA within the zoomed region. Both model versions have 19 sigma-pressure layers extending from the surface up to about 3.8 hPa, corresponding to a vertical resolution of about 300–500 m in the planetary boundary layer (first level at 70 m height) and about 2 km at the tropopause (with 7–9 levels located in the stratosphere) (Hauglustaine et al., 2004). Vertical diffusion and deep convection are parameterized following the schemes of Louis (1979) and Tiedtke (1989), respectively. The simulated horizontal wind vectors (*u* and *v*) are nudged towards the 6-hourly European Center for Medium Range Weather Forecast (ECMWF) reanalysis dataset (ERA-I) in order to simulate the observed large scale advection (Hourdin and Issartel, 2000).

The atmospheric concentrations of hydroxyl radicals (OH), the main sink of atmospheric CH_4, are produced from a simulation at a horizontal resolution of 3.75° in longitude (i.e., 96 model grids) and 1.9° in latitude (i.e., 95 model grids) with the full INCA tropospheric photochemistry scheme (Folberth et al., 2006; Hauglustaine et al., 2004, 2014). The OH fields are climatological monthly data, and are interpolated onto the regular and zoomed model grids, respectively. The magnitude of the OH fields are scaled globally in order that the interannual variation of the simulated CH_4 growth rate agrees well with the observed value (GLOBALVIEW-CH4, 2009). It should be noted that the spatiotemporal distributions of the OH concentrations have large uncertainties and vary greatly among different chemical transport models, therefore the choice of the OH fields may affect the evaluation for CH_4 (especially in terms of the annual gradients between stations and the seasonal cycles). In this study, as we focus more on the improvement of model performance gained from refinement of the horizontal resolution rather than model-observation misfits, the influences of OH variations are assumed to be very small given that the OH fields for both ZASIA and REG are interpolated from a lower model resolution and thus don't show much difference between the two model versions.

The CH_4 and CO_2 concentrations are simulated over the period 2000–2013 with both REG and ZASIA. The first six years (2000–2005) of the simulations are considered as model spin-up, thus we only compared the simulated CH_4 and CO_2 concentrations with observations during 2006–2013. The spin-up time of 6 years may appear short for CH_4 given the ~9-year lifetime of CH_4 in the atmosphere, but simulations are started in 2000 from an initial state

Atmos. Chem. Phys. Discuss., doi:10.5194/acp-2016-1056, 2017
Manuscript under review for journal Atmos. Chem. Phys.
Discussion started: 7 March 2017

with already realistic and almost balanced atmosphere between sources and sinks. The time step of model outputs is hourly.

2.1.2 Prescribed CH_4 and CO_2 surface fluxes

The prescribed CH_4 and CO_2 surface fluxes used as model inputs are presented in Table 1. We simulate the CH_4 concentration fields using a combination of the following datasets: (1) the interannually varing anthropogenic emissions obtained from the Emission Database for Global Atmospheric Research (EDGAR) v4.2 FT2010 product (http://edgar.jrc.ec.europa.eu), including emissions from rice cultivation with the seasonal variations based on Matthews et al. (1991) imposed to the original yearly data; (2) climatogical wetland emissions based on the scheme developed by Kaplan et al. (2006); (3) interannually and seasonally varying biomass burning emissions from Global Fire Emissions Database (GFED) v3.0 product (van der Werf et al., 2010; http://www.globalfiredata.org/data.html), (4) climatological termite emissions (Sanderson, 1996), (5) climatological ocean emissions (Lambert and Schmidt, 1993), and (6) climatological soil uptake (Ridgwell et al., 1999). Based on these emission fields, the global CH_4 emissions in 2010 are 550 $TgCH_4$/yr, and 194 $TgCH_4$/yr over the zoomed region. For the years over which CH_4 anthropogenic emissions (namely, the years 2011–2013) and biomass burning emissions (the years 2012–2013) were not available from the data sources when the simulations were performed, we use emissions for the years 2010 and 2011 respectively.

The prescribed CO_2 fluxes used to simulate the concentration fields are based on the following datasets: (1) three variants (hourly, daily, and monthly means) of interannually varying fossil fuel emissions produced by the Institut für Energiewirtschaft und Rationelle Energieanwendung (IER), Universität Stuttgart on the basis of EDGARv4.2 product (hereafter IER-EDGAR, http://carbones.ier.uni-stuttgart.de/wms/index.html) (Pregger et al., 2007); (2) interannually and seasonally varying biomass burning emission from GFEDv3.1 (van der Werf et al., 2010; http://www.globalfiredata.org/data.html); (3) interannually and hourly varying terrestrial biospheric fluxes produced from outputs of the Organizing Carbon and Hyrology in Dynamic EcosystEm (ORCHIDEE) model; and (4) interannually and seasonally varying air-sea CO_2 gas exchange maps developed by NOAA's Pacific Marine Environmental Laboratory (PMEL) and Atlantic Oceanographic and Meteorological Laboratory (AOML) groups (Park et al., 2010). Here ORCHIDEE runs with the trunk version r1882 (source code available at https://forge.ipsl.jussieu.fr/orchidee/browser/trunk#ORCHIDEE with the revision number of r1882), using the same simulation protocol as the SG3 simulation in MsTMIP project (Huntzinger et al., 2013). The climate forcing data are obtained from CRUNCEP v5.3.2, while the yearly land use maps, soil map and other forcing data (e.g., monthly CO_2 concentrations) are as described in Wei et al. (2014). The sum of global net CO_2 surface fluxes in 2010 are 6.9 PgC/yr, and 3.9 PgC/yr over the zoomed region. Like for CH_4, we use CO_2 biomass burning emissions in the year 2011 to represent emissions in the years 2012 and 2013. For the CO_2 fossil fuel emissions, the IER-EDGAR product is only available until 2009. To generate the emission maps for the years 2010–2013, we scaled the emission spatial distribution in 2009 using the global totals for these years based on the EDGAR v4.2 FT2010 datasets. The detailed information for each surface flux is listed in Table 1.

2.2 Atmospheric CH_4 and CO_2 observations

The simulated CH_4 and CO_2 concentrations are evaluated against observations from 20 flask and 13 continuous surface stations within and around the zoomed region (Figure 1), operated by different programs and organizations (Table 2). The stations where flask observations are published (12 stations) mainly belong to the cooperative program organized by the NOAA Earth System Research Laboratory (NOAA/ESRL, available at ftp://aftp.cmdl.noaa.gov/data/trace_gases/). We also use flask observations from stations operated by China Meterological Administration (CMA, China) (the JIN, LIN and LON stations, see also Fang et al., 2014), Commonwealth Scientific and Research Organization (CSIRO, Australia) (the CRI station, Bhattacharya et al., 2009, available at http://ds.data.jma.go.jp/gmd/wdcgg/), Indian Institute of Tropical Meteorology (IITM, India) (the SNG station, see also Tiwari et al., 2014), and stations from the Indo-French cooperative research program (the HLE, PON and PBL stations, Lin et al., 2015; Swathi et al., 2013). All the CH_4 (CO_2) flask measurements are reported on or linked to the NOAA2004 (WMOX2007) calibration scale, which guarantees comparability between stations in terms of annual means.

The continuous CH_4 and CO_2 measurements are obtained from 13 stations operated by Korea Meteorological Administration (KMA, Korea) (the AMY, GSN and KIS stations), Aichi Air Environment Division (AAED, Japan) (the MKW station), Japan Meteorological Agency

(JMA) (the MNM, RYO and YON stations), National Institute for Environmental Studies (NIES, Japan) (the COI and HAT stations), Agency for Meteorology, Climatology and Geophysics (BMKG, Indonesia) and Swiss Federal Laboratoires for Materials Testing and Research (Empa, Switzerland) (the BKT station). These datasets are available from the World Data Center for Greenhouse Gases (WDCGG, http://ds.data.jma.go.jp/gmd/wdcgg/). Besides, continuous CH_4 and CO_2 measurements are also available from HLE and PON that have been maintained by the Indo-French cooperative research program between LSCE in France and IIA and CSIR4PI in India (Table 2). All the continuous CH_4 (CO_2) measurements used in this study are reported on or traceable to the NOAA2004 (WMOX2007) scale except AMY, COI and HAT. The CO_2 continuous measurements at COI are reported on the NIES95 scale, which is 0.10 to 0.14 ppm lower than WMO in a range between 355 and 385 ppm (Machida et al., 2009). The CH_4 continuous measurements at COI and HAT are reported on the NIES scale, with a conversion factor to WMO scale of 0.9973 (JMA and WMO, 2014). For AMY, the CH_4 measurements over most of the study period are reported on the KRISS scale but they are not traceable to the WMO scale (JMA and WMO, 2014); therefore, we discarded this station from the subsequent analyses of the CH_4 annual gradients between stations. Note that most of the stations where continuous observations are available are located on the east part of the zoomed region, with the exception of HLE, PON and BKT. The stations used in this study span a large range of geographic locations (marine, coastal, mountain or continental) with polluted and non-polluted environments. Both flask and continuous measurements are used to evaluate the model's ability in representing the annual gradient between stations, the seasonal cycle and the synoptic variability for CH_4 and CO_2. The continuous measurements are also used to analyze the diurnal cycle for these two gases.

To evaluate the model performance with regards to vertical transport, we also use observations of the CO_2 vertical profiles from passenger aircraft from the Comprehensive Observation Network for TRace gases by AIrLiner (CONTRAIL) project (Machida et al., 2008, http://www.cger.nies.go.jp/contrail/index.html). This dataset provides high-frequency CO_2 measurements made by on-board continuous CO_2 measuring equipments (CMEs) during commercial airflights between Japan and other Asian countries. The CONTRAIL data are reported on the NIES95 scale, which is 0.10 to 0.14 ppm lower than WMO in a range between 355 and 385 ppm (Machida et al., 2009). In this study, we select from the CONTRAIL dataset all the CO_2 vertical profiles over SEA during the ascending and descending flights for the period 2006–2011, which provided 1808 vertical profiles over a total of 32 airports (Figure S1 and S2).

2.3 Sampling methods and data processing

The model outputs are sampled at the nearest gridpoint and vertical level to each station for both REG and ZASIA. For flask stations, the model outputs are extracted at the exact hour when each flask sample was taken. For continuous stations below 1000 m.a.s.l., since both REG and ZASIA cannot reproduce accurately the nighttime CH_4 and CO_2 accumulation near the ground as in most transport models (Geels et al., 2007), only afternoon (12:00–15:00 LST) data are retained for further analyses of the annual gradients, the seasonal cycle and the synoptic variability. For continuous stations above 1000 m.a.s.l. (only HLE in this study), nighttime (00:00–3:00 LST) data are retained, to avoid sampling local air masses advected by upslope winds from nearby valleys. During daytime, the local valley ascendances and the complex terrain mesoscale circulations cannot be captured by a global transport model.

The curve-fitting routine (CCGvu) developed by NOAA Climate Monitoring and Diagnostic Laboratory (NOAA/CMDL) is applied to the modelled and observed CH_4 and CO_2 time series to extract the annual means, monthly smoothed seasonal cycles and synoptic variations (Thoning et al., 1989). For each station, a smoothed function is fitted to the observed or modelled time series, which consists of a first-order polynomial for the growth rate, two harmonics for the annual cycle (Levin et al., 2002; Ramonet et al., 2002), and a low-pass filter with 80 and 667 days as short-term and long-term cutoff values, respectively (Bakwin et al., 1998). The annual means and the mean seasonal cycle are calculated from the smoothed curve and harmonics, while the synoptic variations are defined as the residuals between the original data and the smoothed fitting curve. Note that we have excluded the observations lying beyond three standard deviations of the residuals around the fitting curve, which are likely to be outliers that are influenced by local fluxes. More detailed descriptions about the curve-fitting procedures and the set-up of parameters can be found in Section 2.3 of Lin et al. (2015).

For the CO_2 vertical profiles from the CONTRAIL passenger aircraft programme, since CO_2 data have been continuously taken every 10 seconds by the onboard CMEs, we average the observed and corresponding simulated CO_2 time series into altitude bins of 1km from the surface to the upper troposphere. We also divide the whole study area into four major subregions for which we group all available CONTRAIL CO_2 profiles (Figure S1), namely East Asia (EAS), the Indian sub-continent (IND), Northern Southeast Asia (NSA) and Southern Southeast Asia (SSA). Given that there are model-observation discrepancies in CO_2 growth rates as well as misfits of absolute CO_2 concentrations, the observed and simulated CONTRAIL time series have been detrended before comparisons of the vertical gradients. To this end, over each subregion, we detrend for each altitude bin the observed and simulated CO_2 time series, by applying the respective linear trend fit to the observed and simulated CO_2 time series of the altitude bin 3–4 km. This altitude bin is thus chosen as reference due to greater data availability compared to other altitudes, and because this level is outside the boundary layer where aircraft CO_2 data are more variable and influenced by local sources (e.g. airports and nearby cities). The detrended CO_2 (denoted as ΔCO_2) referenced to the 3-4 km altitude are seasonally averaged for each altitude bin and each subregion, and the resulting vertical profiles of ΔCO_2 are compared between simulations and observations.

2.4 Metrics

In order to evaluate the model performance to represent observations at different time scales (annual, seasonal, synoptic, diurnal), following Cadule et al. (2010), we define a series of metrics and corresponding statistics for each time scale. All the metrics, defined below, are calculated for both observed and simulated CH_4 (CO_2) time series between 2006 and 2013.

2.4.1 Annual gradients between stations

As inversions use gradients to optimize surface fluxes, it is important to have a metric based upon cross-site gradients. We take Hanle in India (HLE – 78.96°N, 32.78°E, 4517 m a.s.l., Figure 1, Table 2) as a reference and calculate the mean annual gradients by subtracting CH_4 (CO_2) at HLE from those of other stations. HLE is a remote station in the free troposphere within SEA and is located far from any important source/sink areas for both CH_4 and CO_2. These characteristics make HLE an appropriate reference to calculate the gradients between stations. Concentration gradients to HLE are calculated for both observations and model simulations using the corresponding smoothed curves fitted with the CCGvu routine (see Section 2.3). The ability of ZASIA and REG to represent the observed CH_4 (CO_2) annual gradients across all the available stations is quantified by the mean bias (MB, Eq. 1) and the root-mean-square deviation (RMSE, Eq. 2). In Eq. 1 and Eq. 2, m_i and o_i indicate respectively the modelled and observed CH_4 (CO_2) mean annual gradient relative to HLE for a station i.

$$MB = \frac{\sum_{i=1}^{N}(m_i - o_i)}{N} \quad (1)$$

$$RMSE = \sqrt{\frac{\sum_{i=1}^{N}(m_i - o_i)^2}{N}} \quad (2)$$

2.4.2 Seasonal cycle

Two metrics of the model ability to reproduce the observed CH_4 (CO_2) seasonal cycle are considered, the phase and the amplitude. For each station, the seasonal phase is evaluated by the Pearson correlation between the observed and simulated harmonics extracted from the original time series, whereas the seasonal cycle amplitude is evaluated by the ratio of the modelled to the observed seasonal peak-to-peak amplitudes based on the harmonics (A_m / A_o).

2.4.3 Synoptic variability

For each station, the performance of ZASIA and REG to represent the phase (timing) of the synoptic variability is evaluated by the Pearson correlation coefficient between the modelled and observed synoptic deviations (residuals) around the corresponding smoothed fitting curve (see Section 2.3), whereas the performance for the amplitude of the synoptic variability is quantified by the ratio of standard deviations of the residual concentration variability between the model and observations (i.e., Normalized Standard Deviation, NSD, Eq. 3). Further, the overall ability of a model to represent the synoptic variability of CH_4 (CO_2) at a station is quantified by the RMSE (Eq. 4), a metric that can be represented with the Pearson correlation and the NSD in a Taylor diagram (Taylor, 2001). In Eq. 3 and Eq. 4, m_j (o_j) indicates the modelled (observed) synoptic event j, whereas $\overline{m}$ ($\overline{o}$) indicates the arithmetic mean of all the modelled (observed) synoptic events over the study period. Note that for the flask measurements, j corresponds to the time when a flask sample was taken, whereas for the continuous measurements, j corresponds to the early morning (00:00–03:00LST, for mountain stations) or afternoon (12:00–15:00LST, for coastal or island stations) period of each sampling day.

Atmos. Chem. Phys. Discuss., doi:10.5194/acp-2016-1056, 2017
Manuscript under review for journal Atmos. Chem. Phys.
Discussion started: 7 March 2017

$$NSD = \frac{\sqrt{\frac{\sum_{j=1}^{N}\left(m_j-\bar{m}\right)^2}{N}}}{\sqrt{\frac{\sum_{j=1}^{N}\left(o_j-\bar{o}\right)^2}{N}}} \tag{3}$$

$$RMSE = \sqrt{\frac{\sum_{j=1}^{N}\left(m_j-o_j\right)^2}{N}} \tag{4}$$

2.4.4 Diurnal cycle

For each station, the model's ability to reproduce the mean CH_4 (CO_2) diurnal cycle phase in a month is evaluated by the correlation of the hourly mean composite modeled and observed values. With respect to the diurnal cycle amplitude, the model performance strongly varies with stations and seasons, and we do not use a specific metric to evaluate it.

3 Results and discussions

3.1 Annual gradients

3.1.1 CH_4 annual gradients

The annual mean gradient between a station and the HLE reference station relates to the time integral of transport of sources/sinks within the regional footprint area of the station on top of the background gradient caused by remote sources. For CH_4, Figure 2a,b shows the scatterplot of the simulated and observed mean annual gradients to HLE for all stations. In general, both REG and ZASIA capture the signs of the observed CH_4 gradients with reference to HLE, and the simulated gradients roughly distribute around the identity line (Figure 2a,b). The linear regression slope of the simulated versus observed gradients is 1.05±0.08 for ZASIA ($p<0.001$, $R^2=0.88$) against 1.15±0.10 ($p<0.001$, $R^2=0.85$) for REG. The capability of ZASIA in representing the CH_4 gradients is thus slightly better than REG within the zoomed region, with the mean bias and RMSE of -1.2±13.9 and 13.6 ppb for ZASIA, compared to -5.4±20.1 and 20.3 ppb for REG (Table S1; Figure 2a,b). A better performance of ZASIA compared to REG for the CH_4 gradients within SEA is also found for all seasons (Figure S3), with the gradients in summer (AMJ and JAS) being generally better captured than those in winter (OND and JFM). Outside the zoomed region, ZASIA does not perform worse than REG, despite its degraded resolution.

Atmos. Chem. Phys. Discuss., doi:10.5194/acp-2016-1056, 2017
Manuscript under review for journal Atmos. Chem. Phys.
Discussion started: 7 March 2017

When looking into the model performance for different station types, we note that ZASIA performs better for reproducing the gradients vs. HLE at most marine, coastal and continental stations within the zoom region, with a substantial reduction of RMSE compared to that derived from REG (Table S1). In particular, with ZASIA, an improvement of the model performance on the CH_4 annual gradient is found at Shangdianzi (SDZ – 117.12°E, 40.65°N, 293m a.s.l.) and Pondicherry (PON – 79.86°E, 12.01°N, 30m a.s.l.) (for flask measurements), followed by Cape Rama (CRI – 73.83°E, 15.08°N, 66m a.s.l.) (Figure 2a,b), each having an average bias reduction of 36.1 (98.6%), 30.5 (89.9%), 10.6 (74.2%) ppb respectively compared to REG. This improvement may result from a reduction in representation error with a higher model horizontal resolution in the zoomed region, through a better description of the surface fluxes and/or transport around these stations. Particularly, given the presence of large CH_4 emission hotspots in the surface emission maps (Figure S4), ZASIA makes the simulated CH_4 fields more heterogeneous around emission hotspots with finer model grids (e.g., North China in Figure S5), having the potential to better represent stations nearby on an annual basis if the surface fluxes are prescribed with sufficient accuracy (see Figure S6 for SDZ). Besides, stations located in complex terrains (e.g. coastal stations) are more likely to be well characterized with a higher horizontal resolution, as shown in Figure S6 for PON and CRI.

However, a finer grid may also enhance model-data misfits related to inaccurate meteorological forcings and/or surface flux maps. For example, for the coastal station Tae-ahn Peninsula in Korea (TAP – 126.13°E, 36.73°N, 21m a.s.l.), both ZASIA and REG overestimate the observed CH_4 gradients vs. HLE by more than +15 ppb, and ZASIA does worse than REG (Figure S6). The overall poor model performance at this station suggests that emission sources in the prescribed surface flux map are probably overestimated nearby (also see the marine station GSN, Figure S6), although the uncertainty of OH distribution could also play a role. Furthermore, as the CH_4 fields simulated with ZASIA are very sensitive to large emission hotspots (Figure S5), representation of stations near hotspots highly depends on the accuracy of the hotspot location and intensity in the surface emission maps. For Ulaan Uul in Mongolia (UUM – 111.10°E, 44.45°N, 1012m a.s.l.), the existence of the large hotspot (a coal mine) nearby in the EDGARv4.2FT2010 is uncertain, as it is not represented in other inventories like the Regional Emission inventory in ASia (REASv2.1; Kurokawa et al., 2013) (Figure S4). We find that ZASIA does not improve the representation of the observed CH_4 gradients between UUM and HLE (Figure S6), probably due to the

Atmos. Chem. Phys. Discuss., doi:10.5194/acp-2016-1056, 2017
Manuscript under review for journal Atmos. Chem. Phys.
Discussion started: 7 March 2017

presence of this (uncertain) hotspot in the prescribed surface emission maps. Besides, as stated in several previous studies looking at the variability of tracers over continental areas (Geels et al., 2007; Law et al., 2008; Patra et al., 2008), for a station located in a complex terrain (e.g. coastal or mountain sites), the selection of an appropriate gridpoint and/or model level to represent an observation is challenging. In this study we sample the gridpoint and model level nearest to the location of the station, which may not be the best representation of flask data sampling selection strategy (e.g. marine sector at coastal stations or strong winds) and could contribute to the model-observation misfits.

3.1.2 CO_2 annual gradients

For CO_2, both ZASIA and REG are generally able to capture the mean annual gradients between stations, although not as well as for CH_4 (Figure 2c,d). The linear regression slopes between the simulated and the observed gradients are 0.63±0.10 ($p<0.001$, $R^2=0.56$) and 0.65±0.10 ($p<0.001$, $R^2=0.59$) for ZASIA and REG, respectively. Note that both ZASIA and REG are not able to reproduce the CO_2 gradients at tropical stations like Bukit Kototabang in Western Indonesia (BKT – 100.32°E, 0.20°S, 869m a.s.l.), Lulin in Taiwan (LLN – 120.87°E, 23.47°N, 2867m a.s.l.), and SNG and CRI in Western India, with mean biases (absolute value) ranging between 2.5–6.3 ppm, compared to 0.0–1.9 ppm at other sites within the zoomed region (except TAP, see details below). For BKT, the model-observation discrepancies are probably due to imperfect NEE fluxes and/or fire emissions in the prescribed surface fluxes. For SNG and CRI, the significant negative biases of models found during the Northeast monsoon season (October–March) may suggest an underestimation of CO_2 sources in the upwind regions (Figure S7e-h). Figure 2 also shows that, in contrast with CH_4, ZASIA does not significantly improve the representation of CO_2 gradients for stations within the zoomed region, with the mean bias and RMSE close to those of REG. At TAP, ZASIA even degrades model performance (Figure S8), possibly related to misrepresentation of CO_2 sources in the prescribed surface flux map and transport effects. If the ZASIA output is sampled one grid offshore from TAP, the modelled CO_2 gradients become more consistent with observations (Figure S8).

3.1.3 CH_4 vs CO_2

With ZASIA, the model improvement to represent the GHG gradients is more apparent for CH_4 than for CO_2. This difference points towards the quality of source fields for CO_2, and especially natural ones. They are spatially more diffuse than those of CH_4, and temporally more variable in response to weather changes (Parazoo et al., 2008; Wang et al., 2007). Therefore, the regional differences of NEE in SEA not captured by the global ORCHIDEE model may explain the worse fit of the CO_2 gradients compared to CH_4 in both ZASIA and REG. Further, the spatial resolution of the prescribed flux maps may also account for the different model performance for CO_2 and CH_4 (e.g. the spatial resolution of the anthropogenic emissions is 1° for CO_2 and 0.1° for CH_4 respectively). Therefore, with our setup of surface fluxes (Table 1), ZASIA is more likely to resolve the spatial heterogeneity of CH_4 fields, and its improvement over REG is more apparent than that for CO_2. Note that for CO_2, simulations have been performed with the fossil fuel and NEE fluxes that are variable at monthly, daily and hourly scales, respectively. Results show that accounting for daily or hourly variability of fossil CO_2 emissions and NEE fluxes produces almost the same mean annual CO_2 gradients as the simulations prescribed with monthly constant fluxes in each emitting grid-cell. This indicates that the synoptic and diurnal variations of the fossil fuel emissions and NEE from the current ORCHIDEE outputs do not have strong impacts on representation of the mean annual gradients. In the rest of this paper we only present the results driven by hourly fossil fuel emissions and NEE.

3.2 Seasonal cycles

3.2.1 CH_4 seasonal cycles

The model performance for the seasonal cycle depends on the quality of seasonal surface fluxes, atmospheric transport, and chemistry (for CH_4 only). For CH_4, as shown in Figure 3a, both ZASIA and REG generally capture the CH_4 seasonal phases, with correlation coefficients larger than 0.8 at 19 out of 26 stations (73%) for both model verions. However, they are less capable to represent the seasonal cycle at mountain stations, such as Plateau Assy in Kazakhstan (KZM – 77.87°E, 43.25°N, 2524m a.s.l.) (Pearson correlation $R < 0$, not shown in Figure 3a) and Waliguan (WLG – 100.90°E, 36.28°N, 3890m a.s.l.) (Pearson correlation $R < 0.4$, Figure 3a). Compared to REG, ZASIA seems to perform better at elevated stations (see WLG, UUM and probably also SNG in Figure 3a). On the other hand, for stations where the CH_4 seasonal phases are already well simulated, ZASIA does not significantly improve the model performance over REG. For stations ouside the zoomed region (e.g., GMI, COI, RYO), the performance of REG is better given the degraded model resolution.

With respect to the CH_4 seasonal amplitude, for 10 out of 26 stations (inside the dotted circle in Figure 3b), the amplitude ratio ${A_m}/{A_o}$ is within the range 0.75–1.25 for both ZASIA and REG. Among the four station types (symbols with different colors in Figure 3b), the seasonal amplitudes of marine stations are well represented by both model versions, while the seasonal amplitudes at continental (SDZ, WIS, KZD) and mountain stations (e.g. SNG, KZM) are more difficult to capture. Note that for the stations with the seasonal amplitude ratios ${A_m}/{A_o}$ outside the range 0.75–1.25, ZASIA substantially improves the model performance compared to REG (see stations in the shaded areas in Figure 3b).

At mountain stations, the CH_4 seasonal cycle is less accurately represented than for other station types in both model versions. However, ZASIA moderately improves the model performance in several cases, probably through better resolved topography, surface fluxes and/or horizontal transport. For example, the CH_4 seasonal amplitude is better simulated at HLE by ZASIA, in particular for the summer maximum (Figure S9). Given that HLE is a mid-tropospheric background station with negligible influence from local sources (Lin et al., 2015), the improvement by ZASIA suggests that a finer horizontal grid allows for a better representation of the seasonal transport impacting CH_4 at HLE. However, at WLG and KZM, the improvement of the transport with ZASIA is very limited (Figure S9). Possible reasons that account for the model-observation mismatch at mountain sites could be related to the model sampling strategy, and the accuracy of surface flux maps (e.g. unresolved CH_4 sources in summer or possible emission hotspots near stations) and OH distribution. Moreover, the vertical resolution of both model versions is rather coarse (19 layers), and recent tests with the updated physical parameterizations and increased vertical resolution have shown significant improvement of the model performance on vertical transport (Locatelli et al., 2015).

We also note that the CH_4 seasonal cycle at several continental and coastal stations (e.g., SDZ, TAP and GSN; Figure S9) are also not well captured by both model versions. At SDZ in North China, the CH_4 seasonal amplitude is overestimated by 66 ppb (139%) and by 45 ppb

(94%) in ZASIA and REG respectively, with an overestimated summer maximum (Figure S9). Given that SDZ is influenced by air masses passing over several megacities in North China (Beijing, Tianjin, and Tangshan) in summer (Fang et al., 2016), the overestimation of the summer maximum suggests that the actual CH_4 emissions from this region should be lower than the prescribed values in our simulations, apart from the possible influence of inaccurate OH distribution. In addition, the CH_4 seasonal amplitudes at TAP and GSN in the Korean Pennisula are also overestimated by both model versions, suggesting that the prescribed CH_4 emissions may be overestimated in East Asia as well (particularly China). This is consistent with the analyses of the annual CH_4 gradients (Section 3.1), and further reinforced by results from other independent inventories (e.g., Peng et al., 2016) and inverse modeling (Bergamaschi et al., 2013; Bruhwiler et al., 2014; Thompson et al., 2015).

3.2.2 CO_2 seasonal cycles

The CO_2 seasonal cycle mainly represents the seasonal cycle of NEE from ORCHIDEE convoluted with atmospheric transport. Figure 3c illustrates that both ZASIA and REG are able to capture the CO_2 seasonal phases at most stations. A high correlation (Pearson correlation R > 0.8) is found between the simulated and observed CO_2 harmonics for 25 out of 31 stations. ZASIA does not significantly improve the model performance for most stations where the CO_2 phase is already well represented by REG. We note that neither model versions captures the CO_2 seasonal phase at BKT in western Indonesia, no matter whether the evaluation is performed against flask or continuous measurements. Given that representation of the CH_4 seasonal cycle at BKT was satisfactory (Figure S9 for analyses of flask measurements), the worse model performance for CO_2 suggests inaccurate prescribed surface fluxes for NEE and/or fire emissions.

With respect to the CO_2 seasonal amplitude, 14 out of 31 stations have the amplitude ratios ${A_m}/{A_o}$ ranging 0.75–1.25 from both ZASIA and REG (symbols inside the dotted circle in Figure 3d). For the other stations, both model versions tend to underestimate the CO_2 amplitudes, and ZASIA does not improve the model performance. As for CH_4, both ZASIA and REG do not well capture the CO_2 amplitudes at mountain stations (e.g., SNG, LLN and HLE) and continental stations (e.g. SDZ) compared to other station types (e.g. Figure S10). A likely cause can be the inaccurate estimation of NEE in ORCHIDEE (e.g., Peng et al., 2015).

For mountain stations, transport errors and the model sampling strategy may additionally account for the model-observation discrepancies. As mentioned for the annual gradients (Section 3.1), simulations prescribed with monthly, daily and hourly CO_2 surface fluxes generate nearly the same CO_2 seasonal cycle for each station, indicating that the seasonal changes in the magnitude of the CO_2 diurnal rectification do not significantly modulate the average seasonal cycle.

3.3 Synoptic variability

3.3.1 CH_4 synoptic variability

The day-to-day variability of CH_4 and CO_2 residuals are influenced by the regional distribution of fluxes and atmospheric transport at the synoptic scale. For CH_4, as shown in Figure 4a,b, both ZASIA and REG generally capture the synoptic variability at most stations. Apart from UUM where the model performance is poor possibly due to the wrong hotspot near the site in EDGARv4.2 FT2010 (see UUM in Figure S6), for ZASIA (REG), 63% (59%) stations have correlation coefficients (R) higher than 0.5. Both model versions give an NSD range of 0.5–2.0; at stations where the amplitude is not well captured by REG, ZASIA tends to improve the model performance with NSDs closer to 1 (e.g. stations TAP, WLG, SNG, PON in Figure 4a,b).

Among the four station types, the synoptic variability at marine and coastal stations is better simulated, especially within the zoomed region (Figure 4a,b). Given that the prescribed CH_4 surface fluxes are monthly averages, the overall good model performance at marine and coastal stations suggests that variations in atmospheric transport account for most of the CH_4 synoptic variability at these stations. Two exceptions are GSN and TAP (Figure 4a,b). Both stations are not adequately represented, with the amplitudes overestimated throughout the year, by a factor of 1.2–2.3 (Figure S11). These results, together with the overestimated CH_4 gradients (to HLE) and seasonal amplitudes presented before (see Section 3.1 and Section 3.2), again suggest that the prescribed surface fluxes are overestimated near these two stations. The synoptic variability at mountain stations is also fairly well represented by both model versions except WLG and SNG. At SNG, both the phase and amplitude are not well captured, especially in winter. By contrast, the coastal station CRI nearby is much better represented (Figure 4a,b, Figure S12). Given that the two stations may be influenced by air masses from similar source regions, the representation of vertical transport could be problematic at SNG. Compared to other station types, the synoptic variability at continental stations is more difficult to capture (e.g. SDZ and KZD in Figure 4a,b, and UUM not shown), possibly because of errors in the prescribed surface fluxes or/and error in transport over complex continental terrains. Note that at several stations (as shown in Figure S12 for SNG, SDZ and UUM), there are a few synoptic events that are not realistically simulated with very large model-observation misfits. Caution should be taken when assimilating observations from these stations.

3.3.2 CO_2 synoptic variability

For CO_2, as shown in Figure 4c,d, representation of the synoptic variability is overall not as good as for CH_4. Based on model outputs from ZASIA (REG), only 10% (13%) stations have correlation coefficients (R) higher than 0.5, and the NSD values range 0.3–1.4 (0.3–6.3). ZASIA does not significantly improve over REG. This is also true when one looks into different station types or different seasons (Figure S13). At several tropical stations where the CH_4 synoptic variability is found to be simulated correctly (e.g., BKT and PON, Figure 4, Figure S14), both ZASIA and REG are not able to reproduce the phase of the CO_2 synoptic variability. Given that the transport process is the same for both gases in the model, the overall degraded model performance for CO_2 compared to CH_4 suggests biases in the NEE flux fields from ORCHIDEE. As noted by several previous studies (e.g., Patra et al., 2008), CO_2 fluxes with sufficient accuracy and resolution are indispensable for representing the CO_2 synoptic variability. In this study, the daily to hourly NEE variability does not seem to be well represented in ORCHIDEE, especially in the tropics, hence both ZASIA and REG do not capture the CO_2 synoptic variability at stations strongly influenced by regional land fluxes. Futher, at stations influenced by episodic fire emissions (e.g., BKT, and probably PON and PBL), the monthly averaged biomass burning emissions used in this study may not realistically simulate the CO_2 synoptic variability due to the coarse temporal resolution. Besides, the resolution of the prescribed CO_2 ocean fluxes are also rather coarse, which may additionally account for the relatively poor model performance on the CO_2 synoptic variability compared to CH_4, especially for marine and coastal stations.

3.4 Diurnal cycle

3.4.1 CH_4 diurnal cycle

The diurnal cycles of trace gases are mainly controlled by the co-variations between local fluxes and boundary layer mixing (i.g. the diurnal rectifier effect; Denning et al., 1996). For CH_4, the correlation between the simulated and observed diurnal cycles ranges 0.19–0.64 for ZASIA, and the model performance is generally better than that of REG, especially at stations within the zoomed region (Table S2). However, the values of the correlation coefficients remain low. Apart from AMY and COI where both ZASIA and REG fairly well capture the CH_4 diurnal phase, the model performance at other stations is poor and varies from month to month (Table S2). The same conclusion was reached in a previous study by Patra et al. (2009b), which used the ATCM chemistry transport model to simulate CH_4 concentrations at a horizontal resolution of 2.8°×2.8°. Compared to ATCM in Patra et al. (2009b), ZASIA seems to better represent the CH_4 diurnal cycle at coastal stations (AMY, COI, GSN, HAT, MNM and RYO used in both studies). This improved model performance may be at least partly attributed to a better representation of the coastal topograhy and diurnal changes in the land-sea breeze with the finer horizontal grids.

Here, increasing the horizontal resolution does not improve representation of the CH_4 diurnal cycles, therefore several other aspects may account for the model-observation mismatch. First, the prescribed surface fluxes averaged monthly may not be adequate to resolve the diurnal variations at stations strongly influenced by local and regional sources. For example, as shown in Figure 5a,b, the CH_4 diurnal amplitude at AMY is fairly well simulated in winter but substantially underestimated by both ZASIA and REG in summer. Given that emissions from wetlands and rice paddies nearby should affect its CH_4 signals in summer, and that these emissions are temperature and moisture dependent, the climatological surface fluxes used in this study may not be able to reproduce the CH_4 diurnal cycles. Second, model performance also relies on representation of the diurnal variations of boundary layer mixing in the model. The coarse vertical resolution of the transport model (19 levels) has recently been proved to limit the model's ability to account for various dynamical and physical processes in the planetary boundary layer (Locatelli et al., 2015). Locatelli et al. (2015) showed that the refined vertical resolution, together with the updated physical parameterization on turbulent diffusion and convection, can substantially improve performance of the LMDz model on the diurnal cycle of trace gases. Furthermore, representation of the CH_4 diurnal cycle is even more challenging for mountain stations affected by daytime upslope winds and nighttime subsidence (Griffiths et al., 2014; Pérez-Landa et al., 2007). At BKT, located on an altitude of 869 m a.s.l., both model versions do not capture the CH_4 diurnal cycle well when models are sampled at this altitude. However, the first level of the model show better agreement with the observed diurnal cycle at BKT than the level of the station. (Figure 5c,d). This suggests that the vertical transport around this station may not be well represented by both model versions, including the upslope winds that connect the surface layer to the station.

3.4.2 CO_2 diurnal cycle

For CO_2, the correlation between the simulated and observed diurnal cycle ranges from -0.34 to 0.78 for ZASIA. Compared to REG, ZASIA does not always perform better for stations in the zoomed region; in some instances, its performance is even worse (Table S3). As already mentioned, we believe that this poor performance is due to biases in the diurnal cycle of NEE from ORCHIDEE coupled to biases in the diurnal cycle of vertical transport. For example, at GSN (Figure 6a,b), both ZASIA and REG well capture the timing and amplitude of the CO_2 diurnal cycle in winter but not in summer, underlining importance of the data quality of land surface CO_2 fluxes on the model performance, especially during periods when biospheric uptake and release are active. For stations strongly influenced by local sources, the amplitude of the CO_2 diurnal cycle tends to be underestimated. This is the case for PON (Figure 6c,d) on the southeast coast of India, 8 km north of the city of Pondicherry with a population of more than 240,000 in 2011 (Lin et al., 2015). On the one hand, both ZASIA and REG do not adequately capture the diurnal rectifier effect (Denning et al., 1996), since the diurnal cycle of the prescribed NEE fluxes is underestimated and the boundary layer mixing is not well represented by the current model (Locatelli et al., 2015). On the other hand, given that local sources are unresolved in the prescribed CO_2 emissions at 1°×1° resolution, and that the boundary layer air is not well-mixed during nighttime, neither model version captures the CO_2 daily maxima. Again at BKT, as noted for the CH_4 diurnal cycle, we also find better model-observation agreement for the CO_2 diurnal cycle when sampling the first model layer rather than the one corresponding to the station height (Figure 6e,f). Overall, ZASIA does not significantly improve the representation of the CO_2 diurnal cycle (Table S3), even when hourly CO_2 fossil fuel and NEE fluxes are prescribed.

Atmos. Chem. Phys. Discuss., doi:10.5194/acp-2016-1056, 2017
Manuscript under review for journal Atmos. Chem. Phys.
Discussion started: 7 March 2017

3.5 Evaluation against the CONTRAIL CO_2 vertical profiles

Figure 7 shows the simulated and observed CO_2 vertical profiles averaged for different seasons and over different regions. Over East Asia (EAS; Figure 7a and Figure S1), both ZASIA and REG reasonably reproduce the shape of the observed CO_2 vertical profiles. During April–June (AMJ), despite a well-simulated CO_2 vertical profile, the modelled ΔCO_2 (see Section 2.3 for details) are consistently lower than the observations by about 2–3 ppm throughout all altitude bins, possibly due to earlier spring CO_2 uptake simulated by ORCHIDEE in East Asia (also see the CO_2 seasonal cycle at GSN and KIS in Figure S10). The simulated CO_2 vertical gradients between planetary boundary layer (BL) and free troposphere (FT) are lower than the observations by 1–2 ppm during the winter seasons (Figure 8a), possibly due to stronger vertical mixing in LMDz (Locatelli et al., 2015; Patra et al., 2011) as well as flux uncertainty. Note that as most samples (79%) are taken over the Narita International Airport (NRT) and Chubu Centrair International Airport (NGO) in Japan, both of which are located outside the zoomed region, REG better reproduces the BL-FT gradients than ZASIA.

Over the Indian sub-continent (IND, Figure 7b), there is large underestimation of the magnitude of ΔCO_2 near the surface by 4–5 ppm during AMJ, July–September (JAS) and October–December (OND). Accordingly, the BL-FT gradient is underestimated by the same magnitude for these periods (Figure 8b). The model-observation discrepancies are probably not only related to uncertainties in the vertical mixing processes, but also to imperfect surface fluxes throughout the development of the Indian summer monsoon system. This result is consistent with the model underestimation of the CO_2 seasonal amplitude at most surface stations in this region (Figure 3d, Figure S10). When considering the CH_4 and CO_2 measurements at the two mountain station HLE (4517 m a.s.l.) and SNG (1600 m a.s.l.) and a coastal station CRI (66 m a.s.l.) in India, both ZASIA and REG well capture the phase of the CH_4 seasonal cycle at all three stations (Figure S9), whereas the CO_2 seasonal phase is not so well simulated, especially at HLE and SNG (Figure S10). The simulated seasonal CO_2 maximum and minimum at the two inland mountain stations are earlier than the observed ones by up to 1–2 months. This implies that the prescribed NEE does not adequately capture the phenology as well as the magnitude of the strong sources and sinks during the pre-monsoon and monsoon seasons over the Indian sub-continent (Valsala et al., 2013), although the vertical transport (including deep convection) over the periods may also not be well represented in the LMDz model.

The CO_2 vertcial profiles over Southeast Asia (including Northern Southeast Asia (NSA) and Southern Southeast Asia (SSA)) are generally well reproduced. However, both ZASIA and REG fail to reproduce the BL-FT gradient of 3–4 ppm in April for NSA, and during August–October for SSA (Figure 8c,d). Apart from errors in the vertical transport and prescribed NEE, inaccurate estimates of biomass burning emissions could also contribute to this model-observation mismatch.

Overall, the CO_2 vertical profiles from the CONTRAIL project are fairly well simulated by ZASIA and REG over SEA, despite underestimation of the BL-FT gradients, particularly over the Indian sub-continent. This model-observation mismatch are due to a mix of imperfect representation of both vertical transport and surface fluxes, and can not be significantly reduced by solely refining the horizontal resolution of the model, as shown by the very similar vertical profiles derived from ZASIA and REG for CO_2. In order to improve the model performance on the vertical profiles of trace gases (especially the gradients near the surface), the vertical resolution of the model should be increased, together with implementation of the updated physical parameterization for e.g. boundary layer mixing and deep convection in the troposphere (Locatelli et al., 2015).

4 Conclusions and implications

We have simulated the 4-D concentration fields of CH_4 and CO_2 over South and East Asia (SEA) using a zoomed chemical transport model ZASIA. We have evaluated the model's ability to simulate the CH_4 and CO_2 variability at multi-annual, seasonal, synoptic and diurnal scales, against flask and continuous measurements from a unique dataset of 30 surface stations. To assess the model performance, CH_4 and CO_2 are also simulated using the same chemical transport model without the zoom (REG). The results show that both ZASIA and REG are generally capable of representing the annual gradients and seasonal cycles of CH_4 and CO_2, with overall better model performance for CH_4 than CO_2. Compared to REG, ZASIA moderately improves representation of the CH_4 gradients and seasonal cycle; for CO_2, the performance of the two model versions do not show a significant difference, suggesting issues with the surface fluxes used. At the synoptic scale, the CH_4 variability is captured

Atmos. Chem. Phys. Discuss., doi:10.5194/acp-2016-1056, 2017
Manuscript under review for journal Atmos. Chem. Phys.
Discussion started: 7 March 2017

Atmospheric Chemistry and Physics Discussions
Open Access

fairly well for most stations, especially marine and coastal stations, while representation of the CO_2 synoptic variability is not as good as CH_4 even when high-frequency (hourly) anthropogenic emissions and NEE fluxes are prescribed. The model's ability to reproduce the CH_4 and CO_2 diurnal cycle is relatively poor except for a few stations, and better representation of the diurnal cycles cannot be achieved solely with a higher horizontal resolution and with the current model setups. The evaluation at different temporal scales and comparisons between different species and model horizontal resolutions have given us information on possible model improvements needed and implications for inverse modeling, which we summarize in the following paragraphs.

First, the performance of the zoomed chemical transport model is moderately better than REG for CH_4 in SEA. The CH_4 measurements from regional stations and high-frequency sampling are generally better represented with a finer horizontal resolution. This improved representation of the CH_4 variability integrates better description of the topography, the transport and/or the CH_4 surface fluxes around stations. Particularly, given the existence of large CH_4 emission hotspots over SEA, the zoomed transport model simulates more heterogeneous CH_4 fields around emission hotspots and improves representation of stations nearby. However, the strong sensitivity of the simulated CH_4 to emission hotspots also means that the performance of the zoomed transport model depends more on the accuracy of the location and the magnitude of emission hotspots in the prescribed surface fluxes than the regular transport model. As representation of emission hotspots are uncertain in the current bottom-up inventories, caution should be taken when one assimilates observations from stations nearby, particularly those that are unrealistically simulated by the transport model (e.g. the cases for the synoptic variability at SDZ and UUM).

Second, the lower model performance for CO_2 compared to CH_4 at all temporal scales suggests that the CO_2 surface fluxes have not been prescribed with sufficient accuracy. This is particularly true for stations in South and Southeast Asia where NEE does not seem to be well simulated by the terrestrial ecosystem model ORCHIDEE. Given that the bottom-up estimates of CO_2 fluxes from emission inventories and ecosystem models often suffer from large uncertainties, high resolution inverse modeling of CO_2 fluxes could help optimally combine information from atmospheric measurements to improve our knowledge of CO_2 fluxes and variabilities.

Atmos. Chem. Phys. Discuss., doi:10.5194/acp-2016-1056, 2017
Manuscript under review for journal Atmos. Chem. Phys.
Discussion started: 7 March 2017

Third, the performance of the zoomed transport model should be further enhanced by refining the vertical resolution as well as by improving representation of the vertical transport. With the current setups of model layers and physical parameterizations, improvement of model performance is not apparent on hourly to weekly timescales. In addition to improving data quality of the prescribed surface fluxes, the low vertical resolution also limits the models' ability to represent the CH_4 and CO_2 variability at short timescales. In order to take advantage of high-frequency observations at stations close to source regions, it is recommended to increase the model vertical resolution and to improve representation of boundary layer mixing. Such efforts are ongoing with LMDz but will be implemented soon.

Lastly, the model-observation comparisons at multiple temporal scales have the potential to inform us about the magnitude of sources and sinks in the studied region. For example, at GSN, TAP and SDZ, all of which located in East and Northeast Asia, the CH_4 annual gradients as well as the amplitudes of seasonal and synoptic variability are consistently overestimated, suggesting that the prescribed CH_4 emissions in East Asia are overestimated. Atmospheric inversions that assimilate information from these stations are expected to decrease emissions in East Asia, which we will further investigate in future inversion studies.

Atmos. Chem. Phys. Discuss., doi:10.5194/acp-2016-1056, 2017
Manuscript under review for journal Atmos. Chem. Phys.
Discussion started: 7 March 2017

Atmospheric Chemistry and Physics Discussions

Acknowledgement

This study was initiated within the framework of CaFICA-CEFIPRA project (2809-1). X. Lin acknowledges the PhD funding support from AIRBUS Defense & Space. P. Ciais thanks the ERC SyG project IMBALANCE-P 'Effects of Phosphorus Limitations on Life, Earth System and Society' Grant agreement (no. 610028). N. Evangeliou acknowledges the Nordic Center of Excellence eSTICC project (eScience Tools for Investigating Climate Change in northern high latitudes) funded by Nordforsk (no. 57001). We acknowledge the WDCGG for providing the archives of surface station observations for CO_2 and CH_4. We thank the following networks or institutes for the efforts on surface GHG measurements and their access: NOAA/ESRL, Aichi, BMKG, CMA, CSIR4PI, CSIRO, Empa, ESSO/NIOT, IIA, IITM, JMA, KMA, LSCE, NIER, NIES, PU and Saitama. Finally, we would like to thank F. Marabelle and his team at LSCE, and the CURIE (TGCC) platform for the computing support.

References

Aalto, T., Hatakka, J., Karstens, U., Aurela, M., Thum, T. and Lohila, A.: Modeling atmospheric CO_2 concentration profiles and fluxes above sloping terrain at a boreal site, Atmos. Chem. Phys., 6(2), 303–314, doi:10.5194/acp-6-303-2006, 2006.

Aalto, T., Hatakka, J. and Lallo, M.: Tropospheric methane in northern Finland: seasonal variations, transport patterns and correlations with other trace gases, Tellus B, 59(2), 251–259, doi:10.1111/j.1600-0889.2007.00248.x, 2007.

Bakwin, P. S., Tans, P. P., Hurst, D. F. and Zhao, C.: Measurements of carbon dioxide on very tall towers: results of the NOAA/CMDL program, Tellus B, 50(5), 401–415, doi:10.1034/j.1600-0889.1998.t01-4-00001.x, 1998.

Berchet, A., Pison, I., Chevallier, F., Paris, J.-D., Bousquet, P., Bonne, J.-L., Arshinov, M. Y., Belan, B. D., Cressot, C., Davydov, D. K., Dlugokencky, E. J., Fofonov, A. V, Galanin, A., Lavrič, J., Machida, T., Parker, R., Sasakawa, M., Spahni, R., Stocker, B. D. and Winderlich, J.: Natural and anthropogenic methane fluxes in Eurasia: a mesoscale quantification by generalized atmospheric inversion, Biogeosciences, 12(18), 5393–5414, doi:10.5194/bg-12-5393-2015, 2015.

Bergamaschi, P., Corazza, M., Karstens, U., Athanassiadou, M., Thompson, R. L., Pison, I., Manning, A. J., Bousquet, P., Segers, A., Vermeulen, A. T., Janssens-Maenhout, G., Schmidt, M., Ramonet, M., Meinhardt, F., Aalto, T., Haszpra, L., Moncrieff, J., Popa, M. E., Lowry, D., Steinbacher, M., Jordan, A., O'Doherty, S., Piacentino, S. and Dlugokencky, E.: Top-down estimates of European CH_4 and N_2O emissions based on four different inverse models, Atmos. Chem. Phys., 15(2), 715–736, doi:10.5194/acp-15-715-2015, 2015.

Bergamaschi, P., Houweling, S., Segers, A., Krol, M., Frankenberg, C., Scheepmaker, R. A., Dlugokencky, E., Wofsy, S. C., Kort, E. A., Sweeney, C., Schuck, T., Brenninkmeijer, C., Chen, H., Beck, V. and Gerbig, C.: Atmospheric CH_4 in the first decade of the 21st century: Inverse modeling analysis using SCIAMACHY satellite retrievals and NOAA surface measurements, J. Geophys. Res. Atmos., 118(13), 7350–7369, doi:10.1002/jgrd.50480, 2013.

Bergamaschi, P., Krol, M., Dentener, F., Vermeulen, A., Meinhardt, F., Graul, R., Ramonet, M., Peters, W. and Dlugokencky, E. J.: Inverse modelling of national and European CH_4 emissions using the atmospheric zoom model TM5, Atmos. Chem. Phys., 5(9), 2431–2460, doi:10.5194/acp-5-2431-2005, 2005.

Bergamaschi, P., Krol, M., Meirink, J. F., Dentener, F., Segers, A., van Aardenne, J., Monni, S., Vermeulen, A. T., Schmidt, M., Ramonet, M., Yver, C., Meinhardt, F., Nisbet, E. G., Fisher, R. E., O'Doherty, S. and Dlugokencky, E. J.: Inverse modeling of European CH_4 emissions 2001–2006, J. Geophys. Res. Atmos., 115(D22), D22309, doi:10.1029/2010JD014180, 2010.

Bhattacharya, S. K., Borole, D. V, Francey, R. J., Allison, C. E., Steele, L. P., Krummel, P., Langenfelds, R., Masarie, K. A., Tiwari, Y. K. and Patra, P. K.: Trace gases and CO_2 isotope records from Cabo de Rama, India, Curr. Sci., 97(9), 1336–1344, 2009.

Biraud, S., Ciais, P., Ramonet, M., Simmonds, P., Kazan, V., Monfray, P., O'Doherty, S., Spain, T. G. and Jennings, S. G.: European greenhouse gas emissions estimated from continuous atmospheric measurements and ^{222}Radon at Mace Head, Ireland, J. Geophys. Res. Atmos., 105(D1), 1351–1366, doi:10.1029/1999JD900821, 2000.

Boden, T. A., Marland, G. and Andres, R. J.: Global, Regional, and National Fossil-Fuel CO_2 Emissions, Oak Ridge, Tenn., USA., 2015.

Bousquet, P., Ciais, P., Miller, J. B., Dlugokencky, E. J., Hauglustaine, D. A., Prigent, C., Van der Werf, G. R., Peylin, P., Brunke, E.-G., Carouge, C., Langenfelds, R. L., Lathiere, J., Papa, F., Ramonet, M., Schmidt, M., Steele, L. P., Tyler, S. C. and White, J.: Contribution of anthropogenic and natural sources to atmospheric methane variability, Nature, 443(7110), 439–443 [online] Available from: http://dx.doi.org/10.1038/nature05132, 2006.

Bousquet, P., Peylin, P., Ciais, P., Le Quéré, C., Friedlingstein, P. and Tans, P. P.: Regional changes in carbon dioxide fluxes of land and oceans since 1980, Science (80-.)., 290(5495), 1342–1346 [online] Available from: http://science.sciencemag.org/content/290/5495/1342.abstract, 2000.

Bruhwiler, L., Dlugokencky, E., Masarie, K., Ishizawa, M., Andrews, A., Miller, J., Sweeney, C., Tans, P. and Worthy, D.: CarbonTracker-CH_4: an assimilation system for estimating emissions of atmospheric methane, Atmos. Chem. Phys., 14(16), 8269–8293, doi:10.5194/acp-14-8269-2014, 2014.

Cadule, P., Friedlingstein, P., Bopp, L., Sitch, S., Jones, C. D., Ciais, P., Piao, S. L. and Peylin, P.: Benchmarking coupled climate-carbon models against long-term atmospheric CO_2 measurements, Global Biogeochem. Cycles, 24(2), GB2016, doi:10.1029/2009GB003556, 2010.

Chen, Y.-H. and Prinn, R. G.: Atmospheric modeling of high- and low-frequency methane observations: Importance of interannually varying transport, J. Geophys. Res. Atmos., 110(D10), D10303, doi:10.1029/2004JD005542, 2005.

Chevillard, A., Karstens, U. T. E., Ciais, P., Lafont, S. and Heimann, M.: Simulation of atmospheric CO_2 over Europe and western Siberia using the regional scale model REMO, Tellus B, 54(5), 872–894, doi:10.1034/j.1600-0889.2002.01340.x, 2002.

Denning, A. S., Randall, D. A., Collatz, G. J. and Sellers, P. J.: Simulations of terrestrial carbon metabolism and atmospheric CO_2 in a general circulation model, Tellus B, 48(4), 543–567, doi:10.1034/j.1600-0889.1996.t01-1-00010.x, 1996.

Dlugokencky, E. J., Steele, L. P., Lang, P. M. and Masarie, K. A.: Atmospheric methane at Mauna Loa and Barrow observatories: Presentation and analysis of in situ measurements, J. Geophys. Res. Atmos., 100(D11), 23103–23113, doi:10.1029/95JD02460, 1995.

Fang, S., Tans, P. P., Dong, F., Zhou, H. and Luan, T.: Characteristics of atmospheric CO_2 and CH_4 at the Shangdianzi regional background station in China, Atmos. Environ., 131, 1–8, doi:http://dx.doi.org/10.1016/j.atmosenv.2016.01.044, 2016.

Fang, S. X., Zhou, L. X., Tans, P. P., Ciais, P., Steinbacher, M., Xu, L. and Luan, T.: In situ measurement of atmospheric CO_2 at the four WMO/GAW stations in China, Atmos. Chem. Phys., 14(5), 2541–2554, doi:10.5194/acp-14-2541-2014, 2014.

Feng, L., Palmer, P. I., Yang, Y., Yantosca, R. M., Kawa, S. R., Paris, J.-D., Matsueda, H. and Machida, T.: Evaluating a 3-D transport model of atmospheric CO_2 using ground-based, aircraft, and space-borne data, Atmos. Chem. Phys., 11(6), 2789–2803, doi:10.5194/acp-11-2789-2011, 2011.

Folberth, G. A., Hauglustaine, D. A., Lathière, J. and Brocheton, F.: Interactive chemistry in the Laboratoire de Météorologie Dynamique general circulation model: model description

Atmos. Chem. Phys. Discuss., doi:10.5194/acp-2016-1056, 2017
Manuscript under review for journal Atmos. Chem. Phys.
Discussion started: 7 March 2017

and impact analysis of biogenic hydrocarbons on tropospheric chemistry, Atmos. Chem. Phys., 6(8), 2273–2319, doi:10.5194/acp-6-2273-2006, 2006.

Ganesan, A. L., Chatterjee, A., Prinn, R. G., Harth, C. M., Salameh, P. K., Manning, A. J., Hall, B. D., Mühle, J., Meredith, L. K., Weiss, R. F., O'Doherty, S. and Young, D.: The variability of methane, nitrous oxide and sulfur hexafluoride in Northeast India, Atmos. Chem. Phys., 13(21), 10633–10644, doi:10.5194/acp-13-10633-2013, 2013.

Geels, C., Doney, S. C., Dargaville, R., Brandt, J. and Christensen, J. H.: Investigating the sources of synoptic variability in atmospheric CO_2 measurements over the Northern Hemisphere continents: a regional model study, Tellus B, 56(1), 35–50, doi:10.1111/j.1600-0889.2004.00084.x, 2004.

Geels, C., Gloor, M., Ciais, P., Bousquet, P., Peylin, P., Vermeulen, A. T., Dargaville, R., Aalto, T., Brandt, J., Christensen, J. H., Frohn, L. M., Haszpra, L., Karstens, U., Rödenbeck, C., Ramonet, M., Carboni, G. and Santaguida, R.: Comparing atmospheric transport models for future regional inversions over Europe – Part 1: mapping the atmospheric CO2 signals, Atmos. Chem. Phys., 7(13), 3461–3479, doi:10.5194/acp-7-3461-2007, 2007a.

Geels, C., Gloor, M., Ciais, P., Bousquet, P., Peylin, P., Vermeulen, A. T., Dargaville, R., Aalto, T., Brandt, J., Christensen, J. H., Frohn, L. M., Haszpra, L., Karstens, U., Rödenbeck, C., Ramonet, M., Carboni, G. and Santaguida, R.: Comparing atmospheric transport models for future regional inversions over Europe – Part 1: mapping the atmospheric CO_2 signals, Atmos. Chem. Phys., 7(13), 3461–3479, doi:10.5194/acp-7-3461-2007, 2007b.

GLOBALVIEW-CH4: Cooperative Atmospheric Data Integration Project - Methane. CD-ROM., 2009.

Griffiths, A. D., Conen, F., Weingartner, E., Zimmermann, L., Chambers, S. D., Williams, A. G. and Steinbacher, M.: Surface-to-mountaintop transport characterised by radon observations at the Jungfraujoch, Atmos. Chem. Phys., 14(23), 12763–12779, doi:10.5194/acp-14-12763-2014, 2014.

Gurney, K. R., Law, R. M., Denning, A. S., Rayner, P. J., Baker, D., Bousquet, P., Bruhwiler, L., Chen, Y.-H., Ciais, P., Fan, S., Fung, I. Y., Gloor, M., Heimann, M., Higuchi, K., John, J., Maki, T., Maksyutov, S., Masarie, K., Peylin, P., Prather, M., Pak, B. C., Randerson, J., Sarmiento, J., Taguchi, S., Takahashi, T. and Yuen, C.-W.: Towards robust regional estimates of CO_2 sources and sinks using atmospheric transport models, Nature, 415(6872), 626–630 [online] Available from: http://dx.doi.org/10.1038/415626a, 2002.

Haszpra, L.: Carbon dioxide concentration measurements at a rural site in Hungary, Tellus B, 47(1–2), 17–22, doi:10.1034/j.1600-0889.47.issue1.3.x, 1995.

Hauglustaine, D. A., Balkanski, Y. and Schulz, M.: A global model simulation of present and future nitrate aerosols and their direct radiative forcing of climate, Atmos. Chem. Phys., 14(20), 11031–11063, doi:10.5194/acp-14-11031-2014, 2014.

Hauglustaine, D. A., Hourdin, F., Jourdain, L., Filiberti, M.-A., Walters, S., Lamarque, J.-F. and Holland, E. A.: Interactive chemistry in the Laboratoire de Météorologie Dynamique general circulation model: Description and background tropospheric chemistry evaluation, J. Geophys. Res. Atmos., 109(D4), D04314, doi:10.1029/2003JD003957, 2004.

Hourdin, F. and Issartel, J.-P.: Sub-surface nuclear tests monitoring through the CTBT Xenon Network, Geophys. Res. Lett., 27(15), 2245–2248, doi:10.1029/1999GL010909, 2000.

Atmos. Chem. Phys. Discuss., doi:10.5194/acp-2016-1056, 2017
Manuscript under review for journal Atmos. Chem. Phys.
Discussion started: 7 March 2017

Atmospheric Chemistry and Physics
Discussions

Hourdin, F., Musat, I., Bony, S., Braconnot, P., Codron, F., Dufresne, J.-L., Fairhead, L., Filiberti, M.-A., Friedlingstein, P., Grandpeix, J.-Y., Krinner, G., LeVan, P., Li, Z.-X. and Lott, F.: The LMDZ4 general circulation model: climate performance and sensitivity to parametrized physics with emphasis on tropical convection, Clim. Dyn., 27(7–8), 787–813, doi:10.1007/s00382-006-0158-0, 2006.

Houweling, S., Badawy, B., Baker, D. F., Basu, S., Belikov, D., Bergamaschi, P., Bousquet, P., Broquet, G., Butler, T., Canadell, J. G., Chen, J., Chevallier, F., Ciais, P., Collatz, G. J., Denning, S., Engelen, R., Enting, I. G., Fischer, M. L., Fraser, A., Gerbig, C., Gloor, M., Jacobson, A. R., Jones, D. B. A., Heimann, M., Khalil, A., Kaminski, T., Kasibhatla, P. S., Krakauer, N. Y., Krol, M., Maki, T., Maksyutov, S., Manning, A., Meesters, A., Miller, J. B., Palmer, P. I., Patra, P., Peters, W., Peylin, P., Poussi, Z., Prather, M. J., Randerson, J. T., Röckmann, T., Rödenbeck, C., Sarmiento, J. L., Schimel, D. S., Scholze, M., Schuh, A., Suntharalingam, P., Takahashi, T., Turnbull, J., Yurganov, L. and Vermeulen, A.: Iconic CO2 Time Series at Risk, Science (80-.)., 337(6098), 1038–1040 [online] Available from: http://science.sciencemag.org/content/337/6098/1038.2.abstract, 2012.

Huntzinger, D. N., Schwalm, C., Michalak, A. M., Schaefer, K., King, A. W., Wei, Y., Jacobson, A., Liu, S., Cook, R. B., Post, W. M., Berthier, G., Hayes, D., Huang, M., Ito, A., Lei, H., Lu, C., Mao, J., Peng, C. H., Peng, S., Poulter, B., Riccuito, D., Shi, X., Tian, H., Wang, W., Zeng, N., Zhao, F. and Zhu, Q.: The North American Carbon Program Multi-Scale Synthesis and Terrestrial Model Intercomparison Project – Part 1: Overview and experimental design, Geosci. Model Dev., 6(6), 2121–2133, doi:10.5194/gmd-6-2121-2013, 2013.

JMA and WMO: WMO WDCGG Data Summary (WDCGG No. 38) Volume IV - Greenhouse Gases and other Atmospheric Gases. [online] Available from: http://ds.data.jma.go.jp/gmd/wdcgg/pub/products/summary/sum38/sum38.pdf, 2014.

Kaplan, J. O., Folberth, G. and Hauglustaine, D. A.: Role of methane and biogenic volatile organic compound sources in late glacial and Holocene fluctuations of atmospheric methane concentrations, Global Biogeochem. Cycles, 20(2), GB2016, doi:10.1029/2005GB002590, 2006.

Krol, M., Houweling, S., Bregman, B., van den Broek, M., Segers, A., van Velthoven, P., Peters, W., Dentener, F. and Bergamaschi, P.: The two-way nested global chemistry-transport zoom model TM5: algorithm and applications, Atmos. Chem. Phys., 5(2), 417–432, doi:10.5194/acp-5-417-2005, 2005.

Kurokawa, J., Ohara, T., Morikawa, T., Hanayama, S., Janssens-Maenhout, G., Fukui, T., Kawashima, K. and Akimoto, H.: Emissions of air pollutants and greenhouse gases over Asian regions during 2000–2008: Regional Emission inventory in ASia (REAS) version 2, Atmos. Chem. Phys., 13(21), 11019–11058, doi:10.5194/acp-13-11019-2013, 2013.

Lambert, G. and Schmidt, S.: Reevaluation of the oceanic flux of methane: Uncertainties and long term variations, Chemosphere, 26(1–4), 579–589, doi:http://dx.doi.org/10.1016/0045-6535(93)90443-9, 1993.

Law, R. M., Peters, W., Rödenbeck, C., Aulagnier, C., Baker, I., Bergmann, D. J., Bousquet, P., Brandt, J., Bruhwiler, L., Cameron-Smith, P. J., Christensen, J. H., Delage, F., Denning, A. S., Fan, S., Geels, C., Houweling, S., Imasu, R., Karstens, U., Kawa, S. R., Kleist, J., Krol, M. C., Lin, S.-J., Lokupitiya, R., Maki, T., Maksyutov, S., Niwa, Y., Onishi, R., Parazoo, N., Patra, P. K., Pieterse, G., Rivier, L., Satoh, M., Serrar, S., Taguchi, S., Takigawa, M.,

Atmos. Chem. Phys. Discuss., doi:10.5194/acp-2016-1056, 2017
Manuscript under review for journal Atmos. Chem. Phys.
Discussion started: 7 March 2017

Atmospheric Chemistry and Physics
Discussions

Vautard, R., Vermeulen, A. T. and Zhu, Z.: TransCom model simulations of hourly atmospheric CO2: Experimental overview and diurnal cycle results for 2002, Global Biogeochem. Cycles, 22(3), GB3009, doi:10.1029/2007GB003050, 2008.

Law, R. M., Rayner, P. J., Denning, A. S., Erickson, D., Fung, I. Y., Heimann, M., Piper, S. C., Ramonet, M., Taguchi, S., Taylor, J. A., Trudinger, C. M. and Watterson, I. G.: Variations in modeled atmospheric transport of carbon dioxide and the consequences for CO_2 inversions, Global Biogeochem. Cycles, 10(4), 783–796, doi:10.1029/96GB01892, 1996.

Levin, I., Ciais, P., Langenfelds, R., Schmidt, M., Ramonet, M., Sidorov, K., Tchebakova, N., Gloor, M., Heimann, M., Schulze, E.-D., Vygodskaya, N. N., Shibistova, O. and Lloyd, J.: Three years of trace gas observations over the EuroSiberian domain derived from aircraft sampling — a concerted action, Tellus B, 54(5), 696–712, doi:10.1034/j.1600-0889.2002.01352.x, 2002.

Levin, I., Graul, R. and Trivett, N. B. A.: Long-term observations of atmospheric CO_2 and carbon isotopes at continental sites in Germany, Tellus B, 47(1–2), 23–34, doi:10.1034/j.1600-0889.47.issue1.4.x, 1995.

Lin, X., Indira, N. K., Ramonet, M., Delmotte, M., Ciais, P., Bhatt, B. C., Reddy, M. V, Angchuk, D., Balakrishnan, S., Jorphail, S., Dorjai, T., Mahey, T. T., Patnaik, S., Begum, M., Brenninkmeijer, C., Durairaj, S., Kirubagaran, R., Schmidt, M., Swathi, P. S., Vinithkumar, N. V, Yver Kwok, C. and Gaur, V. K.: Long-lived atmospheric trace gases measurements in flask samples from three stations in India, Atmos. Chem. Phys., 15(17), 9819–9849, doi:10.5194/acp-15-9819-2015, 2015.

Locatelli, R., Bousquet, P., Chevallier, F., Fortems-Cheney, A., Szopa, S., Saunois, M., Agusti-Panareda, A., Bergmann, D., Bian, H., Cameron-Smith, P., Chipperfield, M. P., Gloor, E., Houweling, S., Kawa, S. R., Krol, M., Patra, P. K., Prinn, R. G., Rigby, M., Saito, R. and Wilson, C.: Impact of transport model errors on the global and regional methane emissions estimated by inverse modelling, Atmos. Chem. Phys., 13(19), 9917–9937, doi:10.5194/acp-13-9917-2013, 2013.

Locatelli, R., Bousquet, P., Hourdin, F., Saunois, M., Cozic, A., Couvreux, F., Grandpeix, J.-Y., Lefebvre, M.-P., Rio, C., Bergamaschi, P., Chambers, S. D., Karstens, U., Kazan, V., van der Laan, S., Meijer, H. A. J., Moncrieff, J., Ramonet, M., Scheeren, H. A., Schlosser, C., Schmidt, M., Vermeulen, A. and Williams, A. G.: Atmospheric transport and chemistry of trace gases in LMDz5B: evaluation and implications for inverse modelling, Geosci. Model Dev., 8(2), 129–150, doi:10.5194/gmd-8-129-2015, 2015.

Lopez, M., Schmidt, M., Ramonet, M., Bonne, J.-L., Colomb, A., Kazan, V., Laj, P. and Pichon, J.-M.: Three years of semicontinuous greenhouse gas measurements at the Puy de Dôme station (central France), Atmos. Meas. Tech., 8(9), 3941–3958, doi:10.5194/amt-8-3941-2015, 2015.

Louis, J.-F.: A parametric model of vertical eddy fluxes in the atmosphere, Boundary-Layer Meteorol., 17(2), 187–202, doi:10.1007/BF00117978, 1979.

Machida, T., Katsumata, K., Tohjima, Y., Watai, T. and Mukai, H.: Preparing and maintaining of CO_2 calibration scale in National Institute for Environmental Studies: NIES 95 CO_2 scale, in Report of the 14th WMO/IAEA Meeting of Experts on Carbon Dioxide Concentration and Related Tracer Measurement Techniques, edited by T. Laurila, pp. 26–29, GMO/GAW Report No. 186, Helsinki., 2009.

Machida, T., Matsueda, H., Sawa, Y., Nakagawa, Y., Hirotani, K., Kondo, N., Goto, K., Nakazawa, T., Ishikawa, K. and Ogawa, T.: Worldwide measurements of atmospheric CO_2 and other trace gas species using commercial airlines, J. Atmos. Ocean. Technol., 25(10), 1744–1754, doi:10.1175/2008JTECHA1082.1, 2008.

Maksyutov, S., Patra, P. K., Onishi, R., Saeki, T. and Nakazawa, T.: NIES/FRCGC Global Atmospheric Tracer Transport Model: Description, validation, and surfae sources and sinks inversion, J. Earth Simulator, 9, 3–18, 2008.

Matthews, E., Fung, I. and Lerner, J.: Methane emission from rice cultivation: Geographic and seasonal distribution of cultivated areas and emissions, Global Biogeochem. Cycles, 5(1), 3–24, doi:10.1029/90GB02311, 1991.

Miles, N. L., Richardson, S. J., Davis, K. J., Lauvaux, T., Andrews, A. E., West, T. O., Bandaru, V. and Crosson, E. R.: Large amplitude spatial and temporal gradients in atmospheric boundary layer CO_2 mole fractions detected with a tower-based network in the U.S. upper Midwest, J. Geophys. Res. Biogeosciences, 117(G1), n/a-n/a, doi:10.1029/2011JG001781, 2012.

Olivier, J. G. J., Janssens-Maenhout, G., Muntean, M. and Peters, J. A. H. W.: Trends in global CO_2 emissions: 2015 Report., 2015.

Parazoo, N. C., Denning, A. S., Kawa, S. R., Corbin, K. D., Lokupitiya, R. S. and Baker, I. T.: Mechanisms for synoptic variations of atmospheric CO_2 in North America, South America and Europe, Atmos. Chem. Phys., 8(23), 7239–7254, doi:10.5194/acp-8-7239-2008, 2008.

Park, G., Wanninkhof, R. I. F., Doney, S. C., Takahashi, T., Lee, K., Feely, R. A., Sabine, C. L., Triñanes, J. and Lima, I. D.: Variability of global net sea–air CO_2 fluxes over the last three decades using empirical relationships, Tellus B, 62(5), 352–368, doi:10.1111/j.1600-0889.2010.00498.x, 2010.

Patra, P. K., Canadell, J. G., Houghton, R. A., Piao, S. L., Oh, N.-H., Ciais, P., Manjunath, K. R., Chhabra, A., Wang, T., Bhattacharya, T., Bousquet, P., Hartman, J., Ito, A., Mayorga, E., Niwa, Y., Raymond, P. A., Sarma, V. V. S. S. and Lasco, R.: The carbon budget of South Asia, Biogeosciences, 10(1), 513–527, doi:10.5194/bg-10-513-2013, 2013.

Patra, P. K., Houweling, S., Krol, M., Bousquet, P., Belikov, D., Bergmann, D., Bian, H., Cameron-Smith, P., Chipperfield, M. P., Corbin, K., Fortems-Cheiney, A., Fraser, A., Gloor, E., Hess, P., Ito, A., Kawa, S. R., Law, R. M., Loh, Z., Maksyutov, S., Meng, L., Palmer, P. I., Prinn, R. G., Rigby, M., Saito, R. and Wilson, C.: TransCom model simulations of CH4 and related species: linking transport, surface flux and chemical loss with CH_4 variability in the troposphere and lower stratosphere, Atmos. Chem. Phys., 11(24), 12813–12837, doi:10.5194/acp-11-12813-2011, 2011.

Patra, P. K., Law, R. M., Peters, W., Rödenbeck, C., Takigawa, M., Aulagnier, C., Baker, I., Bergmann, D. J., Bousquet, P., Brandt, J., Bruhwiler, L., Cameron-Smith, P. J., Christensen, J. H., Delage, F., Denning, A. S., Fan, S., Geels, C., Houweling, S., Imasu, R., Karstens, U., Kawa, S. R., Kleist, J., Krol, M. C., Lin, S.-J., Lokupitiya, R., Maki, T., Maksyutov, S., Niwa, Y., Onishi, R., Parazoo, N., Pieterse, G., Rivier, L., Satoh, M., Serrar, S., Taguchi, S., Vautard, R., Vermeulen, A. T. and Zhu, Z.: TransCom model simulations of hourly atmospheric CO2: Analysis of synoptic-scale variations for the period 2002–2003, Global Biogeochem. Cycles, 22(4), GB4013, doi:10.1029/2007GB003081, 2008.

Patra, P. K., Takigawa, M., Dutton, G. S., Uhse, K., Ishijima, K., Lintner, B. R., Miyazaki, K.

Atmos. Chem. Phys. Discuss., doi:10.5194/acp-2016-1056, 2017
Manuscript under review for journal Atmos. Chem. Phys.
Discussion started: 7 March 2017

and Elkins, J. W.: Transport mechanisms for synoptic, seasonal and interannual SF_6 variations and “age” of air in troposphere, Atmos. Chem. Phys., 9(4), 1209–1225, doi:10.5194/acp-9-1209-2009, 2009a.

Patra, P., Takigawa, M., Ishijima, K., Choi, B.-C., Cunnold, D., J. Dlugokencky, E., Fraser, P., J. Gomez-Pelaez, A., Goo, T.-Y., Kim, J.-S., Krummel, P., Langenfelds, R., Meinhardt, F., Mukai, H., O’Doherty, S., G. Prinn, R., Simmonds, P., Steele, P., Tohjima, Y., Tsuboi, K., Uhse, K., Weiss, R., Worthy, D. and Nakazawa, T.: Growth rate, seasonal, synoptic, diurnal variations and budget of methane in the lower atmosphere, J. Meteorol. Soc. Japan. Ser. II, 87(4), 635–663, 2009b.

Peng, S., Ciais, P., Chevallier, F., Peylin, P., Cadule, P., Sitch, S., Piao, S., Ahlström, A., Huntingford, C., Levy, P., Li, X., Liu, Y., Lomas, M., Poulter, B., Viovy, N., Wang, T., Wang, X., Zaehle, S., Zeng, N., Zhao, F. and Zhao, H.: Benchmarking the seasonal cycle of CO_2 fluxes simulated by terrestrial ecosystem models, Global Biogeochem. Cycles, 29(1), 46–64, doi:10.1002/2014GB004931, 2015.

Peng, S. S., Piao, S. L., Bousquet, P., Ciais, P., Li, B. G., Lin, X., Tao, S., Wang, Z. P., Zhang, Y. and Zhou, F.: Inventory of anthropogenic methane emissions in Mainland China from 1980 to 2010, Atmos. Chem. Phys. Discuss., 2016, 1–29, doi:10.5194/acp-2016-139, 2016.

Pérez-Landa, G., Ciais, P., Sanz, M. J., Gioli, B., Miglietta, F., Palau, J. L., Gangoiti, G. and Millán, M. M.: Mesoscale circulations over complex terrain in the Valencia coastal region, Spain – Part 1: Simulation of diurnal circulation regimes, Atmos. Chem. Phys., 7(7), 1835–1849, doi:10.5194/acp-7-1835-2007, 2007.

Peters, W., Krol, M. C., Dlugokencky, E. J., Dentener, F. J., Bergamaschi, P., Dutton, G., Velthoven, P. v., Miller, J. B., Bruhwiler, L. and Tans, P. P.: Toward regional-scale modeling using the two-way nested global model TM5: Characterization of transport using SF_6, J. Geophys. Res. Atmos., 109(D19), D19314, doi:10.1029/2004JD005020, 2004.

Peters, W., Krol, M. C., Van Der Werf, G. R., Houweling, S., Jones, C. D., Hughes, J., Schaefer, K., Masarie, K. A., Jacobson, A. R., Miller, J. B., Cho, C. H., Ramonet, M., Schmidt, M., Ciattaglia, L., Apadula, F., Heltai, D., Meinhardt, F., Di Sarra, A. G., Piacentino, S., Sferlazzo, D., Aalto, T., Hatakka, J., StrÖm, J., Haszpra, L., Meijer, H. A. J., Van der Laan, S., Neubert, R. E. M., Jordan, A., RodÓ, X., MorguÍ, J.-A., Vermeulen, A. T., Popa, E., Rozanski, K., Zimnoch, M., Manning, A. C., Leuenberger, M., Uglietti, C., Dolman, A. J., Ciais, P., Heimann, M. and Tans, P. P.: Seven years of recent European net terrestrial carbon dioxide exchange constrained by atmospheric observations, Glob. Chang. Biol., 16(4), 1317–1337, doi:10.1111/j.1365-2486.2009.02078.x, 2010.

Popa, M. E., Gloor, M., Manning, A. C., Jordan, A., Schultz, U., Haensel, F., Seifert, T. and Heimann, M.: Measurements of greenhouse gases and related tracers at Bialystok tall tower station in Poland, Atmos. Meas. Tech., 3(2), 407–427, doi:10.5194/amt-3-407-2010, 2010.

Pregger, T., Scholz, Y. and Friedrich, R.: Documentation of the anthropogenic GHG emission data for Europe provided in the Frame of CarboEurope GHG and CarboEurope IP, Stuttgart, Germany., 2007.

Le Quéré, C., Moriarty, R., Andrew, R. M., Canadell, J. G., Sitch, S., Korsbakken, J. I., Friedlingstein, P., Peters, G. P., Andres, R. J., Boden, T. A., Houghton, R. A., House, J. I., Keeling, R. F., Tans, P., Arneth, A., Bakker, D. C. E., Barbero, L., Bopp, L., Chang, J., Chevallier, F., Chini, L. P., Ciais, P., Fader, M., Feely, R. A., Gkritzalis, T., Harris, I., Hauck, J., Ilyina, T., Jain, A. K., Kato, E., Kitidis, V., Klein Goldewijk, K., Koven, C., Landschützer, P., Lauvset, S. K., Lefèvre, N., Lenton, A., Lima, I. D., Metzl, N., Millero, F., Munro, D. R., Murata, A., Nabel, J. E. M. S., Nakaoka, S., Nojiri, Y., O'Brien, K., Olsen, A., Ono, T., Pérez, F. F., Pfeil, B., Pierrot, D., Poulter, B., Rehder, G., Rödenbeck, C., Saito, S., Schuster, U., Schwinger, J., Séférian, R., Steinhoff, T., Stocker, B. D., Sutton, A. J., Takahashi, T., Tilbrook, B., van der Laan-Luijkx, I. T., van der Werf, G. R., van Heuven, S., Vandemark, D., Viovy, N., Wiltshire, A., Zaehle, S. and Zeng, N.: Global Carbon Budget 2015, Earth Syst. Sci. Data, 7(2), 349–396, doi:10.5194/essd-7-349-2015, 2015.

Ramonet, M., Ciais, P., Nepomniachii, I., Sidorov, K., Neubert, R. E. M., Langendörfer, U., Picard, D., Kazan, V., Biraud, S., Gusti, M., Kolle, O., Schulze, E.-D. and Lloyd, J.: Three years of aircraft-based trace gas measurements over the Fyodorovskoye southern taiga forest, 300 km north-west of Moscow, Tellus B, 54(5), 713–734, doi:10.1034/j.1600-0889.2002.01358.x, 2002.

Ridgwell, A. J., Marshall, S. J. and Gregson, K.: Consumption of atmospheric methane by soils: A process-based model, Global Biogeochem. Cycles, 13(1), 59–70, doi:10.1029/1998GB900004, 1999.

Rödenbeck, C., Houweling, S., Gloor, M. and Heimann, M.: CO_2 flux history 1982–2001 inferred from atmospheric data using a global inversion of atmospheric transport, Atmos. Chem. Phys., 3(6), 1919–1964, doi:10.5194/acp-3-1919-2003, 2003.

Saeki, T., Saito, R., Belikov, D. and Maksyutov, S.: Global high-resolution simulations of CO2 and CH4 using a NIES transport model to produce a priori concentrations for use in satellite data retrievals, Geosci. Model Dev., 6(1), 81–100, doi:10.5194/gmd-6-81-2013, 2013.

Sanderson, M. G.: Biomass of termites and their emissions of methane and carbon dioxide: A global database, Global Biogeochem. Cycles, 10(4), 543–557, doi:10.1029/96GB01893, 1996.

Sasakawa, M., Shimoyama, K., Machida, T., Tsuda, N., Suto, H., Arshinov, M., Davydov, D., Fofonov, A., Krasnov, O., Saeki, T., Koyama, Y. and Maksyutov, S.: Continuous measurements of methane from a tower network over Siberia, Tellus B, 62(5), 403–416, doi:10.1111/j.1600-0889.2010.00494.x, 2010.

Swathi, P. S., Indira, N. K., Rayner, P. J., Ramonet, M., Jagadheesha, D., Bhatt, B. C. and Gaur, V. K.: Robust inversion of carbon dioxide fluxes over temperate Eurasia in 2006-2008, Curr. Sci., 105(2), 201–208, 2013.

Szopa, S., Balkanski, Y., Schulz, M., Bekki, S., Cugnet, D., Fortems-Cheiney, A., Turquety, S., Cozic, A., Déandreis, C., Hauglustaine, D., Idelkadi, A., Lathière, J., Lefevre, F., Marchand, M., Vuolo, R., Yan, N. and Dufresne, J.-L.: Aerosol and ozone changes as forcing for climate evolution between 1850 and 2100, Clim. Dyn., 40(9–10), 2223–2250, doi:10.1007/s00382-012-1408-y, 2013.

Taylor, K. E.: Summarizing multiple aspects of model performance in a single diagram, J. Geophys. Res. Atmos., 106(D7), 7183–7192, doi:10.1029/2000JD900719, 2001.

Thompson, R. L., Ishijima, K., Saikawa, E., Corazza, M., Karstens, U., Patra, P. K., Bergamaschi, P., Chevallier, F., Dlugokencky, E., Prinn, R. G., Weiss, R. F., O'Doherty, S., Fraser, P. J., Steele, L. P., Krummel, P. B., Vermeulen, A., Tohjima, Y., Jordan, A., Haszpra, L., Steinbacher, M., Van der Laan, S., Aalto, T., Meinhardt, F., Popa, M. E., Moncrieff, J. and Bousquet, P.: TransCom N_2O model inter-comparison – Part 2: Atmospheric inversion

Atmos. Chem. Phys. Discuss., doi:10.5194/acp-2016-1056, 2017
Manuscript under review for journal Atmos. Chem. Phys.
Discussion started: 7 March 2017

estimates of N_2O emissions, Atmos. Chem. Phys., 14(12), 6177–6194, doi:10.5194/acp-14-6177-2014, 2014.

Thompson, R. L., Patra, P. K., Chevallier, F., Maksyutov, S., Law, R. M., Ziehn, T., van der Laan-Luijkx, I. T., Peters, W., Ganshin, A., Zhuravlev, R., Maki, T., Nakamura, T., Shirai, T., Ishizawa, M., Saeki, T., Machida, T., Poulter, B., Canadell, J. G. and Ciais, P.: Top-down assessment of the Asian carbon budget since the mid 1990s, Nat Commun, 7 [online] Available from: http://dx.doi.org/10.1038/ncomms10724, 2016.

Thompson, R. L., Stohl, A., Zhou, L. X., Dlugokencky, E., Fukuyama, Y., Tohjima, Y., Kim, S.-Y., Lee, H., Nisbet, E. G., Fisher, R. E., Lowry, D., Weiss, R. F., Prinn, R. G., O'Doherty, S., Young, D. and White, J. W. C.: Methane emissions in East Asia for 2000–2011 estimated using an atmospheric Bayesian inversion, J. Geophys. Res. Atmos., 120(9), 4352–4369, doi:10.1002/2014JD022394, 2015.

Thoning, K. W., Tans, P. P. and Komhyr, W. D.: Atmospheric carbon dioxide at Mauna Loa Observatory: 2. Analysis of the NOAA GMCC data, 1974–1985, J. Geophys. Res. Atmos., 94(D6), 8549–8565, doi:10.1029/JD094iD06p08549, 1989.

Tian, H., Lu, C., Ciais, P., Michalak, A. M., Canadell, J. G., Saikawa, E., Huntzinger, D. N., Gurney, K. R., Sitch, S., Zhang, B., Yang, J., Bousquet, P., Bruhwiler, L., Chen, G., Dlugokencky, E., Friedlingstein, P., Melillo, J., Pan, S., Poulter, B., Prinn, R., Saunois, M., Schwalm, C. R. and Wofsy, S. C.: The terrestrial biosphere as a net source of greenhouse gases to the atmosphere, Nature, 531(7593), 225–228 [online] Available from: http://dx.doi.org/10.1038/nature16946, 2016.

Tiedtke, M.: A Comprehensive mass flux scheme for cumulus parameterization in large-scale models, Mon. Weather Rev., 117(8), 1779–1800, doi:10.1175/1520-0493(1989)117<1779:ACMFSF>2.0.CO, 1989.

Tiwari, Y. K. and Kumar, R. K.: GHG observation programs in India, Asian GAW Greenh. Gases Newsl., No.3, 5–11, 2012.

Tiwari, Y. K., Vellore, R. K., Ravi Kumar, K., van der Schoot, M. and Cho, C.-H.: Influence of monsoons on atmospheric CO_2 spatial variability and ground-based monitoring over India, Sci. Total Environ., 490(0), 570–578, doi:http://dx.doi.org/10.1016/j.scitotenv.2014.05.045, 2014.

Valsala, V., Tiwari, Y. K., Pillai, P., Roxy, M., Maksyutov, S. and Murtugudde, R.: Intraseasonal variability of terrestrial biospheric CO_2 fluxes over India during summer monsoons., J. Geophys. Res. Biogeosciences, 118(2), 752–769, doi:10.1002/jgrg.20037, 2013.

Wada, A., Matsueda, H., Sawa, Y., Tsuboi, K. and Okubo, S.: Seasonal variation of enhancement ratios of trace gases observed over 10 years in the western North Pacific, Atmos. Environ., 45(12), 2129–2137, doi:http://dx.doi.org/10.1016/j.atmosenv.2011.01.043, 2011.

Wang, J.-W., Denning, A. S., Lu, L., Baker, I. T., Corbin, K. D. and Davis, K. J.: Observations and simulations of synoptic, regional, and local variations in atmospheric CO_2, J. Geophys. Res. Atmos., 112(D4), D04108, doi:10.1029/2006JD007410, 2007.

Wang, R., Balkanski, Y., Boucher, O., Ciais, P., Schuster, G. L., Chevallier, F., Samset, B. H., Liu, J., Piao, S., Valari, M. and Tao, S.: Estimation of global black carbon direct radiative forcing and its uncertainty constrained by observations, J. Geophys. Res. Atmos., 121(10), 5948–5971, doi:10.1002/2015JD024326, 2016.

Wang, R., Tao, S., Balkanski, Y., Ciais, P., Boucher, O., Liu, J., Piao, S., Shen, H., Vuolo, M. R., Valari, M., Chen, H., Chen, Y., Cozic, A., Huang, Y., Li, B., Li, W., Shen, G., Wang, B. and Zhang, Y.: Exposure to ambient black carbon derived from a unique inventory and high-resolution model, Proc. Natl. Acad. Sci. [online] Available from: http://www.pnas.org/content/early/2014/01/23/1318763111.abstract, 2014.

Wei, Y., Liu, S., Huntzinger, D. N., Michalak, A. M., Viovy, N., Post, W. M., Schwalm, C. R., Schaefer, K., Jacobson, A. R., Lu, C., Tian, H., Ricciuto, D. M., Cook, R. B., Mao, J. and Shi, X.: The North American Carbon Program Multi-scale Synthesis and Terrestrial Model Intercomparison Project – Part 2: Environmental driver data, Geosci. Model Dev., 7(6), 2875–2893, doi:10.5194/gmd-7-2875-2014, 2014.

van der Werf, G. R., Randerson, J. T., Giglio, L., Collatz, G. J., Mu, M., Kasibhatla, P. S., Morton, D. C., DeFries, R. S., Jin, Y. and van Leeuwen, T. T.: Global fire emissions and the contribution of deforestation, savanna, forest, agricultural, and peat fires (1997–2009), Atmos. Chem. Phys., 10(23), 11707–11735, doi:10.5194/acp-10-11707-2010, 2010.

Winderlich, J., Chen, H., Gerbig, C., Seifert, T., Kolle, O., Lavrič, J. V, Kaiser, C., Höfer, A. and Heimann, M.: Continuous low-maintenance CO_2/CH_4/H_2O measurements at the Zotino Tall Tower Observatory (ZOTTO) in Central Siberia, Atmos. Meas. Tech., 3(4), 1113–1128, doi:10.5194/amt-3-1113-2010, 2010.

Yver Kwok, C., Laurent, O., Guemri, A., Philippon, C., Wastine, B., Rella, C. W., Vuillemin, C., Truong, F., Delmotte, M., Kazan, V., Darding, M., Lebègue, B., Kaiser, C., Xueref-Rémy, I. and Ramonet, M.: Comprehensive laboratory and field testing of cavity ring-down spectroscopy analyzers measuring H_2O, CO_2, CH_4 and CO, Atmos. Meas. Tech., 8(9), 3867–3892, doi:10.5194/amt-8-3867-2015, 2015.

Atmos. Chem. Phys. Discuss., doi:10.5194/acp-2016-1056, 2017
Manuscript under review for journal Atmos. Chem. Phys.
Discussion started: 7 March 2017

Tables

Table 1 The prescribed CH_4 and CO_2 surface fluxes used as model input. For each trace gas, magnitudes of different types of fluxes are given for the year 2010. $Total_{global}$ and $Total_{zoom}$ indicate the total flux summarized over the globe and the zoomed region, respectively.

Type of CH_4 fluxes	Temporal resolution	Spatial resolution	$Total_{global}$ ($TgCH_4$/yr)	$Total_{zoom}$ ($TgCH_4$/yr)	Data source
Anthropogenic – rice	Monthly, interannual	0.1°	38	32	EDGARv4.2FT2010 + Matthews et al (1991)
Anthropogenic – others	Yearly, interannual	0.1°	320	131	EDGARv4.2FT2010
Wetland	Monthly, climatological	1°	175	29	Kaplan et al. (2006)
Biomass burning	Monthly, interannual	0.5°	19	3	GFED v3.0
Termite	Monthly, climatological	1°	19	3	Sanderson et al. (1996)
Soil	Monthly, climatological	1°	-38	-7	Ridgwell et al. (1999)
Ocean	Monthly, climatological	1°	17	3	Lambert & Schmidt (1993)
Total, $TgCH_4$/yr			550	194	
Type of CO_2 fluxes	Temporal resolution	Spatial resolution	$Total_{global}$ (PgC/yr)	$Total_{zoom}$ (PgC/yr)	Data source
Anthropogenic	Monthly, interannual	1°	8.9	3.6	IER-EDGAR product
Anthropogenic	Daily, interannual	1°			
Anthropogenic	Hourly, interannual	1°			
Biomass burning	Monthly, interannual	0.5°	2.0	0.2	GFED v3.1
Land flux (NEE)	Monthly, interannual	0.5°	-2.7	0.1	OCHIDEE outputs from trunk version r1882
Land flux (NEE)	Daily, interannual	0.5°			
Land flux (NEE)	Hourly, interannual	0.5°			
Ocean flux	Monthly, interannual	4°×5°	-1.3	0.1	NOAA/PMEL & AOML product; Park et al. (2010)
Total, PgC/yr			6.9	3.9	

Table 2 Stations used in this study. For the column 'Zoom', 'Y' indicates a station within the zoomed region.

	Code	Station	LON (°)	LAT (°)	Altitude (m a.s.l.)	Contributor	Type	Temporal coverage	Zoom	CH_4	CO_2
1	AMY	Anmyeon-do, Korea	126.32	36.53	133	KMA	coastal	2006–2013	Y	Y	
2	BKT	Bukit Kototabang, Indonesia	100.32	-0.20	869	BMKG, Empa, NOAA/RSRL	coastal	Flask: 2006–2013 CH_4 continuous: 2009–2013 CO_2 continuous: 2010–2013	Y	Y	Y
3	COI	Cape Ochi-ishi, Japan	145.50	43.16	94	NIES	coastal	2006–2013		Y	
4	CRI	Cape Rama, India	73.83	15.08	66	CSIRO	coastal	2009–2013	Y	Y	Y
5	DDR	Mt. Dodaira, Japan	139.18	36.00	840	Saitama	continental	2006–2013			Y
6	DSI	Dongsha Island, Taiwan, China	116.73	20.70	8	National Central Univ., NOAA/ESRL	marine	2010–2013	Y	Y	Y
7	GMI	Mariana Island, Guam	144.66	13.39	5	Univ. of Guam, NOAA/ESRL	marine	2006–2013		Y	Y
8	GSN	Gosan, Korea	126.12	33.15	144	NIER	marine	2006–2011	Y	Y	Y
9	HAT	Hateruma, Japan	123.81	24.06	47	NIES	marine	2006–2013	Y	Y	
10	HLE	Hanle, India	78.96	32.78	4517	LSCE, CSIR4PI, IIA	mountain	Flask: 2006–2013 CH_4 continuous: 2012–2013 CO_2 continuous: 2006–2013	Y	Y	Y
11	JIN	Jinsha, China	114.20	29.63	750	CMA	continental	2006–2011	Y		Y
12	KIS	Kisai - Saitama	139.55	36.08	13	Saitama	continental	2006–2013			Y
13	KZD	Sary Taukum, Kazakhstan	75.57	44.45	412	KSIEMC, NOAA/ESRL	continental	2006–2009	Y	Y	Y
14	KZM	Plateau Assy, Kazakhstan	77.87	43.25	2524	KSIEMC, NOAA/ESRL	mountain	2006–2009	Y	Y	Y
15	LIN	Lin'an, China	119.72	30.30	139	CMA	continental	2006–2011	Y		Y
16	LLN	Lulin, Taiwan, China	120.87	23.47	2867	LAIBS, NOAA/ESRL	mountain	2006–2013	Y	Y	Y
17	LON	Longfengshan, China	127.60	44.73	331	CMA	continental	2006–2011	Y		Y
18	MKW	Mikawa-Ichinomiya, Japan	137.43	34.85	50	Aichi	continental	2006–2011	Y		Y
19	MNM	Minamitori-shima, Japan	153.98	24.28	28	JMA	marine	2006–2013		Y	Y
20	PBL	Port Blair, India	92.76	11.65	20	LSCE, CSIR4PI, ESSO/NIOT	marine	2009–2013	Y	Y	Y
21	PON	Pondicherry, India	79.86	12.01	30	LSCE, CSIR4PI, Pondicherry Univ.	coastal	Flask: 2006–2013 CH_4 continuous: 2011–2013 CO_2 continuous: 2011–2013	Y	Y	Y
22	RYO	Ryori, Japan	141.82	39.03	280	JMA	continental	2006–2013		Y	Y
23	SDZ	Shangdianzi, China	117.12	40.65	293	CMA, NOAA/ESRL	continental	2009–2013	Y	Y	Y
24	SEY	Mahe Island, Seychelles	55.53	-4.68	7	SBS, NOAA/ESRL	marine	2006–2013		Y	Y
25	SNG	Sinhagad, India	73.75	18.35	1600	IITM	mountain	CH_4 flask: 2010–2013	Y	Y	Y

Atmos. Chem. Phys. Discuss., doi:10.5194/acp-2016-1056, 2017
Manuscript under review for journal Atmos. Chem. Phys.
Discussion started: 7 March 2017

								CO_2 flask: 2009–2013			
26	TAP	Tae-ahn Peninsula, Korea	126.13	36.73	21	KCAER, NOAA/ESRL	coastal	2006–2013	Y	Y	Y
27	UUM	Ulaan Uul, Mongolia	111.10	44.45	1012	MHRI, NOAA/ESRL	continental	2006–2013	Y	Y	Y
28	WIS	Negev Desert, Israel	30.86	34.79	482	WIS, AIES, NOAA/ESRL	continental	2006–2013		Y	Y
29	WLG	Mt. Waliguan, China	100.90	36.28	3890	CMA, NOAA/ESRL	mountain	2006–2013	Y	Y	Y
30	YON	Yonagunijima, Japan	123.02	24.47	50	JMA	marine	2006–2013	Y	Y	Y

Abbreviations:
Aichi – Aichi Air Environment Division, Japan
AIES – Arava Institute for Environmental Studies, Israel
BMKG – Agency for Meteorology, Climatology and Geophysics, Indonesia
CMA – China Meteorological Administration, China
CSIR4PI – Council of Scientific and Industrial Research Fourth Paradigm Institute, India
CSIRO – Commonwealth Scientific and Industrial Research Organisation, Australia
Empa – Swiss Federal Laboratories for Materials Testing and Research, Switzerland
ESSO/NIOT – Earth System Sciences Organisation/National Institute of Ocean Technology, India
IIA – Indian Institute of Astrophysics, India
IITM – Indian Institute of Tropical Meteorology, India
JMA – Japan Meteorological Agency, Japan
KCAER – Korea Centre for Atmospheric Environment Research, Republic of Korea
KMA – Korea Meteorological Administration, Republic of Korea
KSIEMC – Kazakh Scientific Institute of Environmental Monitoring and Climate, Kazakhstan
LAIBS – Lulin Atmospheric Background Station, Taiwan
LSCE – Laboratoire des Sciences du Climat et de l'Environnement, France
MHRI – Mongolian Hydrometeorological Research Institute, Mongolia
NIER – National Institute of Environmental Research, South Korea
NIES – National Institute for Environmental Studies, Japan
NIWA – National Institute of Water and Atmospheric Research, New Zealand
NOAA/ESRL – National Oceanic and Atmospheric Administration/Earth System Research Laboratory
Saitama – Center for Environmental Science in Saitama
SBS – Seychelles Bureau of Standards, Seychelles
WIS – Weizmann Institute of Science, Israel

Atmos. Chem. Phys. Discuss., doi:10.5194/acp-2016-1056, 2017
Manuscript under review for journal Atmos. Chem. Phys.
Discussion started: 7 March 2017

Atmospheric Chemistry and Physics
Open Access
Discussions

Figures

Figure 1 Map of locations of stations used in this study. The zoomed grid of the LMDz-INCA model is also plotted with the NASA Shuttle Radar Topographic Mission (SRTM) 1km digital elevation data (DEM) as background (http://srtm.csi.cgiar.org). The grey shaded area indicates the region with a horizontal resolution of 0.66° × 0.51°. The red close circle (blue cross) represents the atmospheric station where flask (in-situ) measurements are available and used in this study.

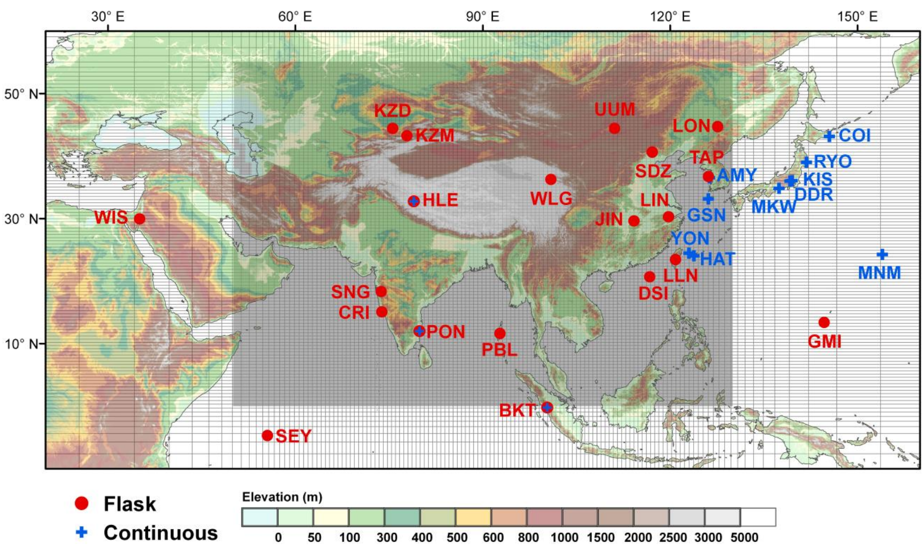

Atmos. Chem. Phys. Discuss., doi:10.5194/acp-2016-1056, 2017
Manuscript under review for journal Atmos. Chem. Phys.
Discussion started: 7 March 2017

Atmospheric Chemistry and Physics
Open Access
Discussions

Figure 2 Scatterplots of simulated and observed mean annual gradients of CH_4 (a, b) or CO_2 (c, d) between HLE and other stations. For both tracers, the simulated gradients are based on simulations from ZASIA (a, c) and REG (b, d). In each panel, the black dotted line indicates the identity line, whereas the grey solid line indicates the linear line fitted to the data. The black (grey) texts give the mean bias (±1σ) and RMSE of the simulated mean annual gradients in reference to the observed ones for stations within (outside) the zoomed region. The italic type and open symbols in the legend denote stations outside the zoomed region.

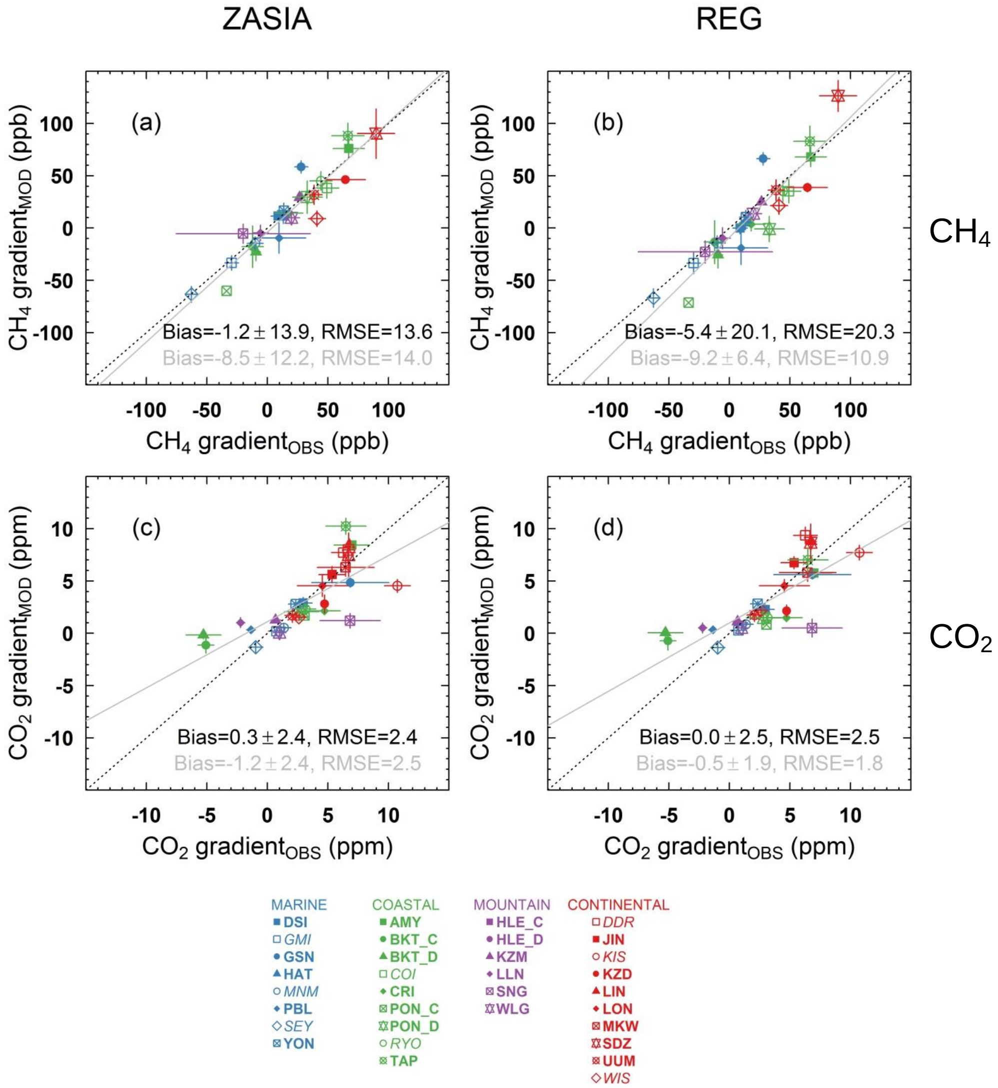

Atmos. Chem. Phys. Discuss., doi:10.5194/acp-2016-1056, 2017
Manuscript under review for journal Atmos. Chem. Phys.
Discussion started: 7 March 2017

Atmospheric Chemistry and Physics
Discussions

Figure 3 (a,c) Correlations between the observed and simulated CH_4 or CO_2 mean seasonal cycles from ZASIA (y axis) and REG (x axis) for all available stations. (b,d) Ratios of the simulated to observed CH_4 or CO_2 seasonal amplitude from ZASIA (y axis) and REG (x axis) for all available stations. Stations within the dotted circles have a ratio of the simulated to observed amplitude ranging 0.75–1.25 from both ZASIA and REG. The grey shaded regions mark the domains where ZASIA better capture the seasonal amplitude than REG. For each station, the mean seasonal cycle is calculated from the harmonics of the corresponding smoothed fitting curve, and the seasonal amplitude is defined as the difference between the seasonal maximum and minimum.

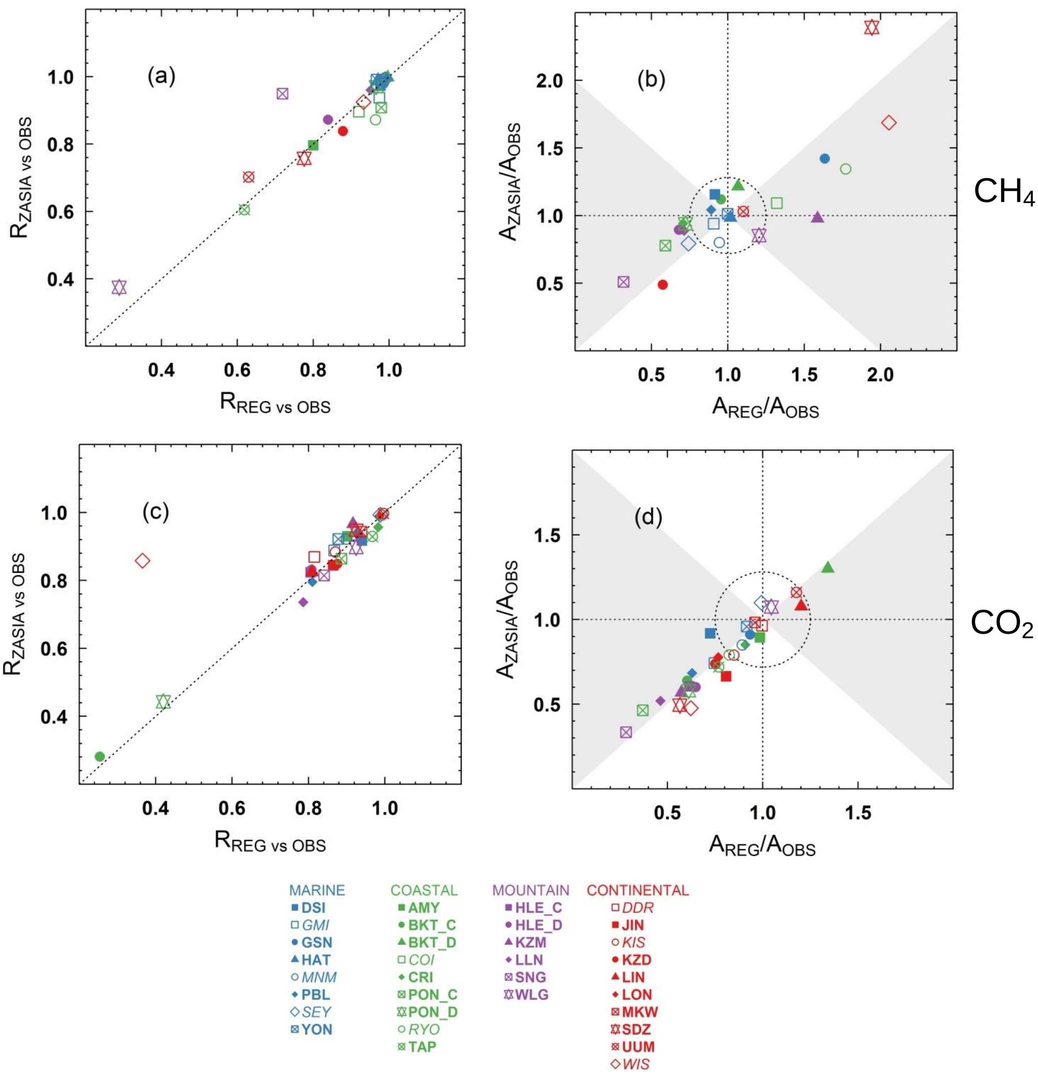

Atmos. Chem. Phys. Discuss., doi:10.5194/acp-2016-1056, 2017
Manuscript under review for journal Atmos. Chem. Phys.
Discussion started: 7 March 2017

Figure 4 Taylor diagrams showing correlations and normalized standard deviations (NSD; the ratio of the simulated to observed standard deviation) between the simulated and observed CH_4 (a,b) or CO_2 (c,d) synoptic variability for all available stations. For each station, the synoptic variability is calculated from residuals from the smoothed fitting curve.

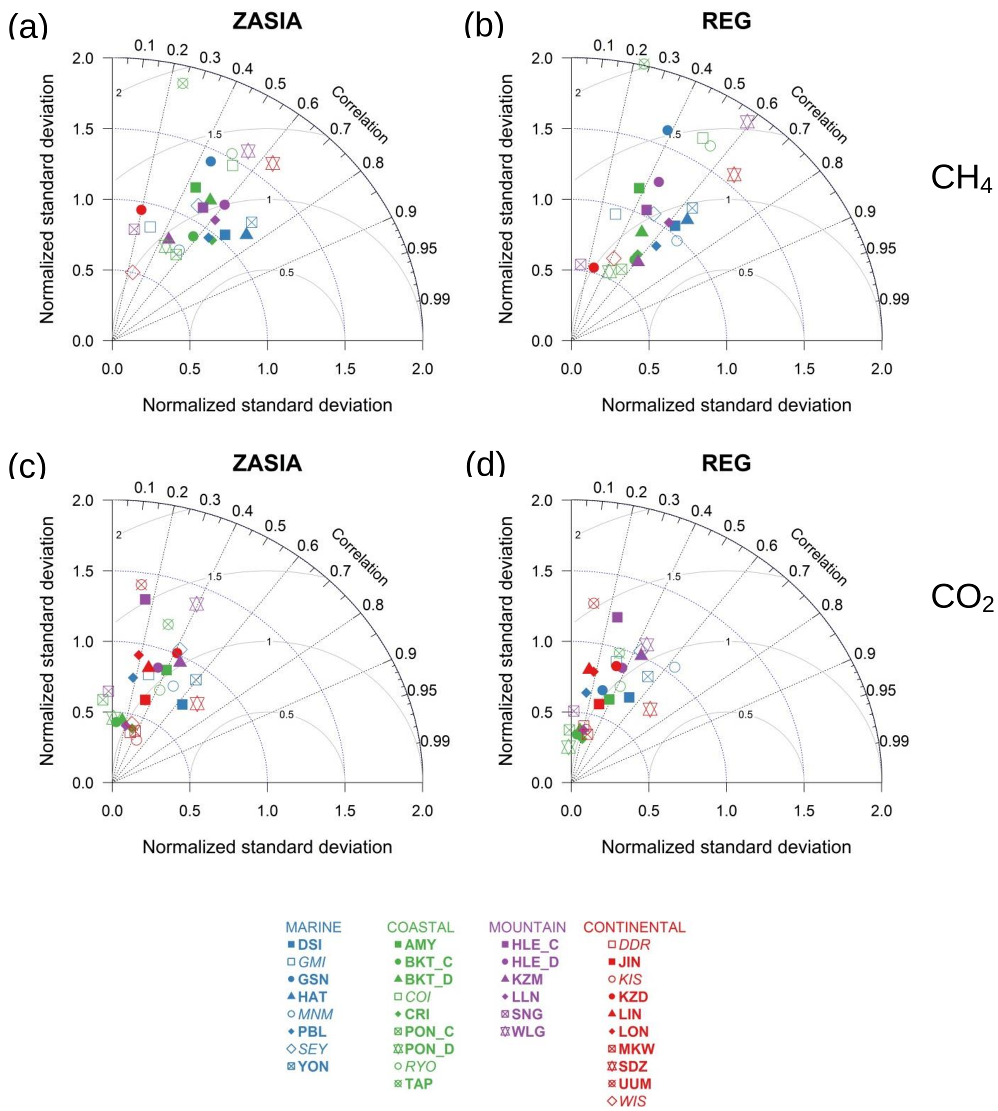

Figure 5 Observed and simulated hourly CH_4 time series for AMY (126.32°E, 36.53°N, 133m a.s.l.) in Korean Peninsula and BKT (100.32°E, 0.20°S, 869m a.s.l.) in Indonesia. For each panel, the black dots indicate the CH_4 measurements, while the red and blue dots indicate the simulated CH_4 time series from ZASIA and REG, respectively. For BKT, we also present the simulated CH_4 time series sampled at the first layer of both versions of the model (colored in purple and green for ZASIA and REG, respectively).

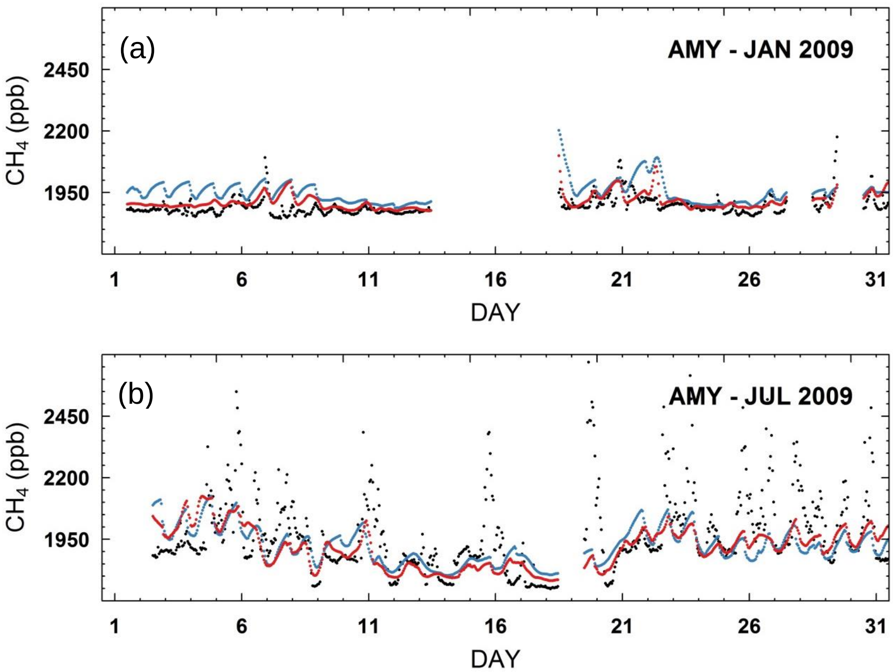

Atmos. Chem. Phys. Discuss., doi:10.5194/acp-2016-1056, 2017
Manuscript under review for journal Atmos. Chem. Phys.
Discussion started: 7 March 2017

Atmospheric Chemistry and Physics
Discussions
Open Access
EGU

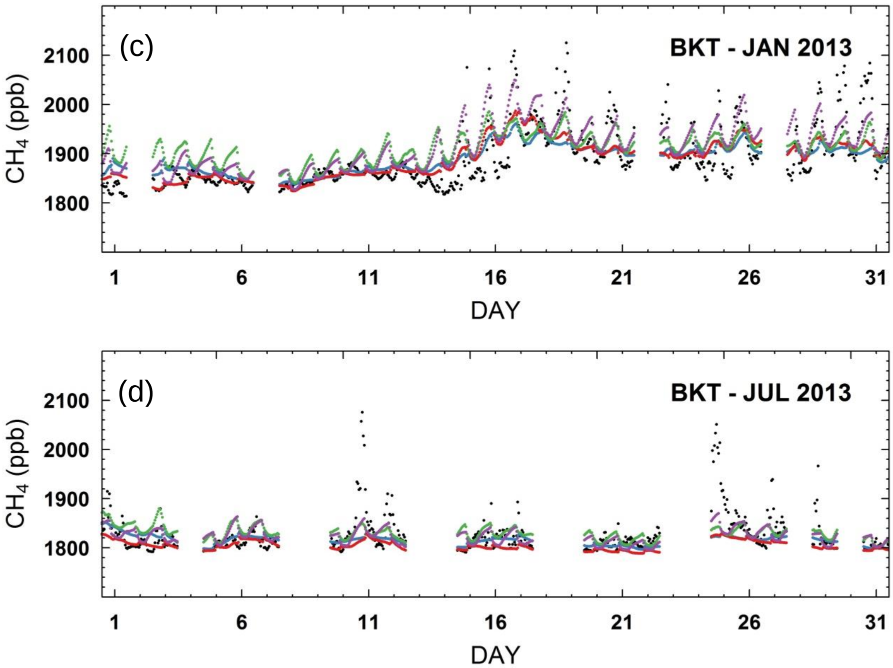

Atmos. Chem. Phys. Discuss., doi:10.5194/acp-2016-1056, 2017
Manuscript under review for journal Atmos. Chem. Phys.
Discussion started: 7 March 2017

Figure 6 Observed and simulated hourly CO_2 time series for GSN (126.12°E, 33.15°N, 144m a.s.l.) in South Korea, PON (79.86°E, 12.01°N, 30m a.s.l.) in India and BKT (100.32°E, 0.20°S, 869m a.s.l.) in Indonesia. For each panel, the black dots indicate the CO_2 measurements, while the red and blue dots indicate the simulated CO_2 time series from ZASIA and REG, respectively. For BKT, we also present the simulated CO_2 time series sampled at the first layer of both models (colored in purple and green for ZASIA and REG, respectively).

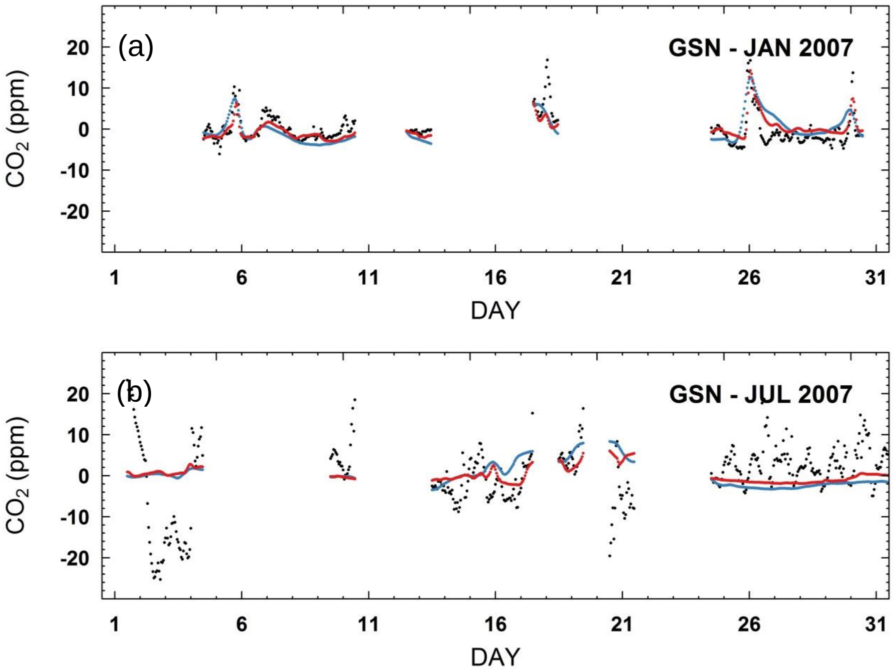

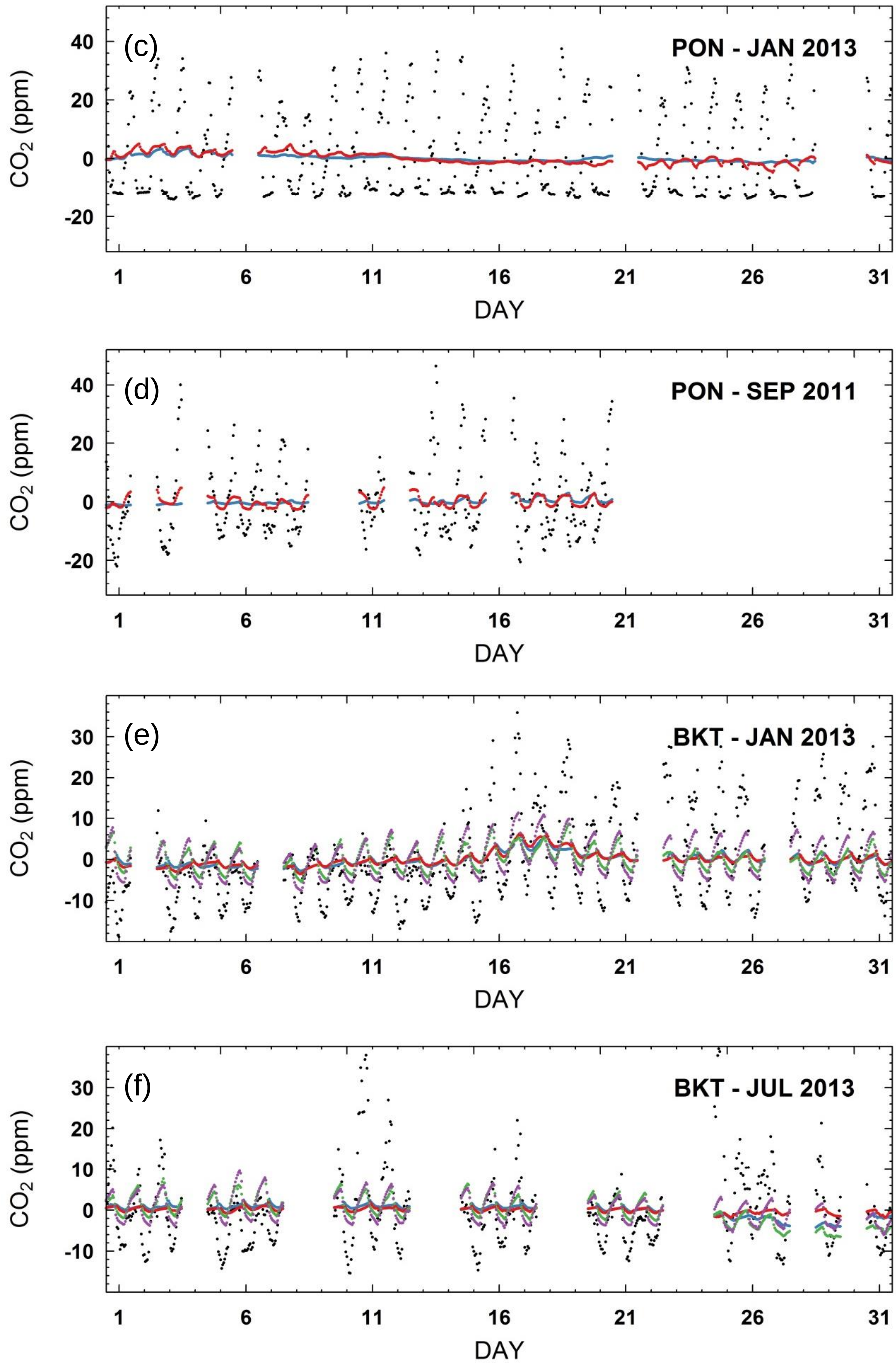
(c)
PON - JAN 2013
(d)
PON - SEP 2011
(e)
BKT - JAN 2013
(f)
BKT - JUL 2013
CO2 (ppm)
DAY
40
20
0
-20
30
10
-10
1
6
11
16
21
26
31

Atmospheric Chemistry and Physics
Open Access
Discussions

Figure 7 Seasonal mean observed and simulated CO_2 vertical profiles over **(a)** East Asia (EAS), **(b)** the Indian sub-continent (IND), **(c)** Northern Southeast Asia (NSA) and **(d)** Southern Southeast Asia (SSA). The observed vertical profiles are based on CO_2 continuous measurements onboard the commercial air flights from the CONTRAIL project during the period 2006–2011. For each 1-km altitude bin and each subregion, the observed and simulated time series are detrended (denoted as ΔCO_2) and seasonally averaged during January–March (JFM), April–June (AMJ), July–September (JAS) and October–December (OND). For each panel, the error bars and shaded areas give the standard deviations of the observed and simulated ΔCO_2 at each altitude bin and within each subregion.

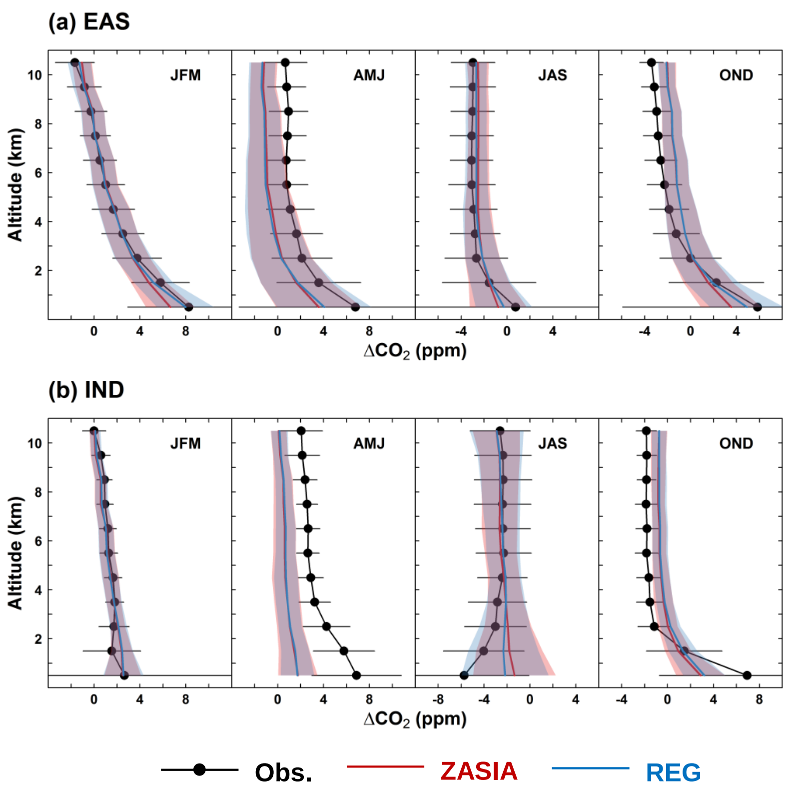

Atmos. Chem. Phys. Discuss., doi:10.5194/acp-2016-1056, 2017
Manuscript under review for journal Atmos. Chem. Phys.
Discussion started: 7 March 2017

Atmospheric Chemistry and Physics
Open Access
Discussions

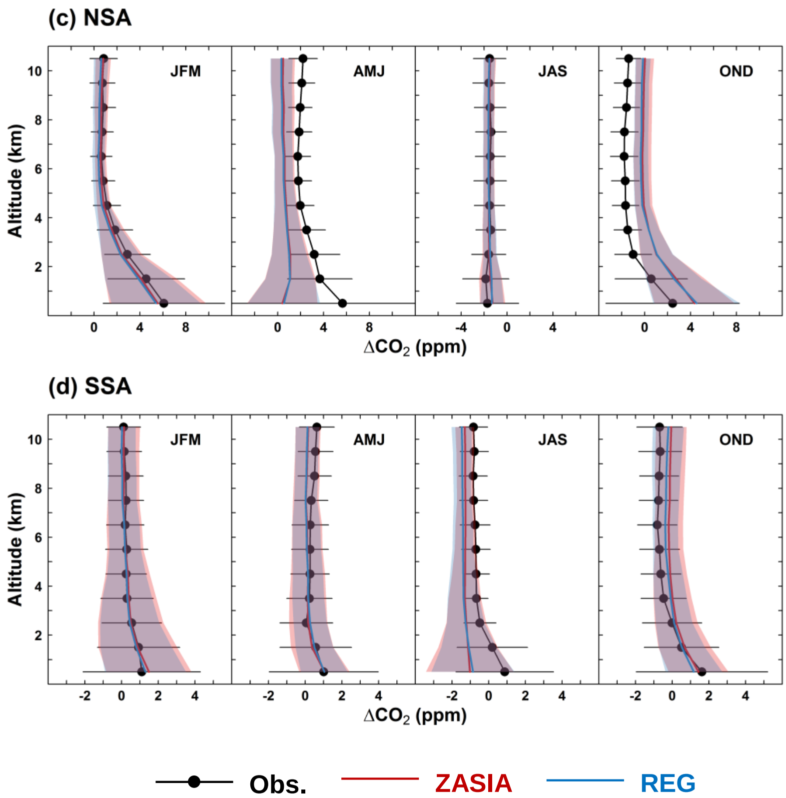

Atmos. Chem. Phys. Discuss., doi:10.5194/acp-2016-1056, 2017
Manuscript under review for journal Atmos. Chem. Phys.
Discussion started: 7 March 2017

Atmospheric Chemistry and Physics
Open Access
Discussions

Figure 8 Monthly mean observed and simulated CO_2 gradient between 1 and 4km over **(a)** East Asia (EAS), **(b)** the Indian sub-continent (IND), **(c)** Northern Southeast Asia (NSA) and **(d)** Southern Southeast Asia (SSA). For each subregion, the monthly CO_2 gradients are calculated by averaging over all the vertical profiles the differences in CO_2 concentrations between 1 and 4km. The error bars and shaded areas indicate the standard deviations of the observed and simulated CO_2 gradients.